Contractile Cell Plasticity in Inherited Cerebral Small Vessel Disease

Timon Landinger

München 2021

Aus dem
Institut für Schlaganfall- und Demenzforschung (ISD)
der Ludwig–Maximilians–Universität München
Direktor: Prof. Dr. med. Martin Dichgans

Contractile Cell Plasticity in Inherited Cerebral Small Vessel Disease

Dissertation
zum Erwerb des Doktorgrades der Medizin
an der Medizinischen Fakultät der
Ludwig–Maximilians–Universität zu München

vorgelegt von
Timon Landinger

aus
München

2021

Mit Genehmigung der Medizinischen Fakultät
der Universität München

Berichterstatter:	PD Dr. rer. nat. Christof Haffner
Mitberichterstatter:	Prof. Dr. Edgar Meinl
	apl. Prof. Dr. Johannes Levin
Mitbetreuung durch die promovierte Mitarbeiterin:	Dr. rer. nat. Nathalie Beaufort
Dekan:	Prof. Dr. med. dent. Reinhard Hickel
Tag der mündlichen Prüfung:	25. März 2021

Eidesstattliche Versicherung

Ich erkläre hiermit an Eides statt,

dass ich die vorliegende Dissertation mit dem Thema

Contractile Cell Plasticity in Inherited Cerebral Small Vessel Disease

selbständig verfasst, mich außer der angegebenen keiner weiteren Hilfsmittel bedient und alle Erkenntnisse, die aus dem Schrifttum ganz oder annähernd übernommen sind, als solche kenntlich gemacht und nach ihrer Herkunft unter Bezeichnung der Fundstelle einzeln nachgewiesen habe. Ich erkläre des Weiteren, dass die hier vorgelegte Dissertation nicht in gleicher oder in ähnlicher Form bei einer anderen Stelle zur Erlangung eines akademischen Grades eingereicht wurde.

München, 30. März 2021

Timon Landinger

Table of Contents

List of Figures

List of Tables

List of Acronyms

To provide better legibility, some long versions of the acronyms listed here may still contain shorter acronyms, all of which are also included in this list.

AD Alzheimer's disease

AFD Anderson-Fabry disease

α-SMA α-smooth muscle actin

BCA bicinchoninic acid

BMP bone morphogenic protein

bp base pairs

BSA bovine serum albumin

C Celsius

CADASIL cerebral autosomal-dominant arteriopathy with subcortical infarcts and leukoencephalopathy

CARASIL cerebral autosomal-recessive arteriopathy with subcortical infarcts and leukoencephalopathy

cDNA complementary DNA

CMB cerebral microbleed

co-SMAD common-mediator SMAD

CSF cerebrospinal fluid

CT computed tomography

CTGF connective tissue growth factor

DAPI 4',6-diamidino-2-phenylindole

ddH_2O double-distilled water

DMEM Dulbecco's modified Eagle's medium

DMSO dimethyl sulfoxide

DNA desoxyribonucleic acid

dNTP deoxynucleoside triphosphate

DTT dithiothreitol

ECM extracellular matrix

EDTA ethylenediaminetetraacetic acid

EMT epithelial–mesenchymal transition

ETS E26 transformation-specific

FCS fetal calf serum

FLAIR fluid-attenuated inversion recovery

GKLF gut-enriched Krueppel-like factor

GOM granular osmiophilic material

GTP guanosine triphosphate

HDAC histone deacetylase

H&E haematoxylin and eosin

HRP horseradish peroxidase

HTRA1 high temperature requirement A 1 serine protease

IGF insulin-like growth factor

IHC immunohistochemistry

kDa kilodalton

kg kilogram

Klf Krueppel-like factor

LDS Loeys-Dietz syndrome

LTBP latent TGF-β binding protein

LTR long terminal repeat

M molar

mg milligram

miRNA micro RNA

MKL myocardin-like protein

mL milliliter

mM millimolar

mm millimeter

MRI magnetic resonance imaging

mRNA messenger RNA

MRTF myocardin-related transcription factor

MTT 3-(4,5-dimethylthiazol-2-yl)-2,5-diphenyltetrazolium bromide

µg microgram

µL microliter

µM micromolar

µm micrometer

ng nanogram

nM nanomolar

nm nanometer

NO nitric oxide

NP40 Tergitol-type NP40 (nonyl-phenoxypolyethoxylethanol)

NRT no reverse transcriptase

NTC no template control

OD optical density

OMIM Online Mendelian Inheritance in Man

PAI plasminogen activator inhibitor

PBS phosphate-buffered saline

PCR polymerase chain reaction

PDGF platelet-derived growth factor

PDGFR-β PDGF receptor β

PFA paraformaldehyde

PVDF polyvinylidene fluoride

qPCR quantitative real-time polymerase chain reaction

RA retinoic acid

RNA ribonucleic acid

RT reverse transcriptase

ROS reactive oxygen species

RT room temperature

R-SMAD receptor-regulated SMAD

RT-qPCR reverse transcription-quantitative real-time PCR

RVCL retinal vasculopathy with cerebral leukodystrophy

s second(s)

SBE SMAD-binding element

SDS sodium dodecyl sulfate

SDS-PAGE SDS-polyacrylamide gel electrophoresis

SEM standard error of the mean

SM22 smooth muscle protein 22-α / transgelin

Smad mothers against decapentaplegic homolog

SM-MHC smooth muscle myosin heavy chain / myosin-11x

SNP	single nucleotide polymorphism
SRE	serum response element
SRF	serum response factor
SVD	cerebral small vessel disease
TBS-T	Tris-buffered saline-Tween
TCE	TGF-β control element
TCF	ternary complex factor
TEMED	tetramethylethylenediamine
TGF-β	transforming growth factor-β
TGFBR	TGF-β-receptor
TREX1	three-prime repair exonuclease 1
Tris	tris(hydroxymethyl)aminomethane
V	Volt
VaD	vascular dementia
VCI	vascular cognitive impairment
VSMC	vascular smooth muscle cell(s)
WB	western blot
WMH	white matter hyperintensities
WT	wild type

1 Summary

Cerebral small vessel disease (SVD) is a major cause of stroke and disability. This is especially true for hereditary forms featuring more severe phenotypes. CARASIL is an early onset familial SVD caused by homozygous mutations in the gene encoding the protease HTRA1. In addition, heterozygous *HTRA1* mutations have recently been shown to cause milder SVD. HTRA1 plays a crucial role in transforming growth factor-β (TGF-β) signaling, which, in turn, regulates cell differentiation, including that of vascular smooth muscle cell(s). However, the molecular and cellular mechanisms that promote HTRA1-related SVD are largely unknown.

In the present study, I used skin fibroblasts from patients bearing homo- or heterozygous *HTRA1* mutations and performed mRNA and protein analysis, as well as contraction assays. I evidenced that HTRA1 loss-of-function correlates with decreased TGF-β signaling activity in heterozygous cells. Moreover, I established that heterozygous patient cells display a downregulation of contractile proteins, a reduced contractile activity and an upregulation of phagocytosis-associated markers, suggesting a disease-related cell phenotype switch from contractile to phagocytic. Accordingly, immunoblot and *in situ* immunohistochemistry both confirmed a reduced contractile marker expression in cerebral vessels of *HTRA1*$^{-/-}$ mice. I identified the transcriptional regulator Klf4 as a putative orchestrator of disease-related cell phenotypic switching and demonstrated that treatment with recombinant TGF-β is sufficient to restore TGF-β signaling and contractile cell function *ex vivo*.

Together, my data provide new insights in the pathomechanisms underlying HTRA1-related SVD.

2 Zusammenfassung

Zerebrale Mikroangiopathien sind bedeutende Ursachen von Schlaganfällen und anderer krankheitsbedingter Lebensqualitätseinbußen. Dies gilt besonders für vererbte Formen, welche überwiegend durch stärker ausgeprägte Krankheitssymptome auffallen. CARASIL ist eine hereditäre zerebrale Mikroangiopathie mit früher Erstmanifestation und wird durch homozygote Mutationen in dem für die Protease HTRA1 codierenden Gen hervorgerufen. In jüngerer Vergangenheit wurden zudem heterozygote Mutationen in *HTRA1* als Ursache von zerebralen Mikroangiopathien schwächeren Phänotyps identifiziert. HTRA1 ist ein wichtiger Bestandteil des TGF-β-Signalweges, der die Differenzierung verschiedener Zelltypen einschließlich glatter Gefäßmuskelzellen reguliert. Die molekularen und zellulären Mechanismen, welche an der Manifestation HTRA1-assoziierter zerebraler Mikroangiopathien beteiligt sind, sind weitestgehend unbekannt.

In der vorliegenden Arbeit führte ich an kultivierten Fibroblasten von Patienten mit homo- bzw. heterozygoten *HTRA1*-Mutationen mRNA- und Proteinanalysen sowie Kontraktionsassays durch. Ich konnte zeigen, dass ein Funktionsverlust von HTRA1 mit einer verminderten TGF-β-Signalaktivität in heterozygoten Zellen einhergeht. Zudem beobachtete ich in diesen Zellen einen Verlust kontraktiler Marker, eine herabgesetzte Kontraktilität, sowie eine vermehrte Expression phagozytoseassoziierter Marker. In der Zusammenschau legen meine Beobachtungen somit eine krankhafte Umdifferenzierung von einem kontraktilen hin zu einem phagozytischen Zellphänotyp nahe. Analog hierzu konnte ich mittels Western Blot und *in situ*-Immunhistochemie eine reduzierte Expression kontraktiler Marker in zerebralen Blutgefäßen HTRA1-defizienter Mäuse nachweisen. Des Weiteren identifizierte

ich den Transkriptionsfaktor Klf4 als mögliches Regulationselement besagter krankhaften Veränderung des Zellphänotyps und zeigte, dass mittels Behandlung mit rekombinantem TGF-β eine suffiziente Wiederherstellung der TGF-β-Signalkaskade sowie der kontraktilen Zellfunktion *ex vivo* erreicht werden kann.

Zusammenfassend gesagt zeigen die Ergebnisse der vorliegenden Arbeit neue Erkenntnisse über die Pathomechanismen, welche der HTRA1-assoziierten zerebralen Mikroangiopathie zugrunde liegen, auf.

3 Introduction

3.1 Cerebral Small Vessel Disease (SVD)

3.1.1 Definition and Epidemiology of SVD

Cerebral small vessel disease (SVD) is characterized by a typical pattern of clinical, neuroimaging and neuropathological findings (Wardlaw et al., 2013) resulting from damage to perforating small arteries and arterioles, which reach from either the subarachnoid circulation or the large basal cerebral arteries into the white matter of the brain (Pantoni, 2010) (Figure 3.1).

SVD is responsible for most cases of hemorrhagic stroke (the most catastrophic type of stroke) and a quarter of ischemic strokes. Consequently, it is a significant cause of disability and death among adults. In addition, SVD is the most frequent cause of vascular cognitive impairment (VCI) and its more severe and advanced stage, vascular dementia (VaD). Either alone or in combination with neurodegenerative pathologies such as Alzheimer's disease (AD), SVD contributes to at least 40 % of dementia cases.

The prevalence of SVD greatly increases with age. Therefore clinical or neuroradiological findings correlated to the disease (see Section 3.1.3) can be observed in approximately 80 % of 65-year-olds and almost all 90-year old individuals (Haffner et al., 2016). Advanced age, hypertension and diabetes are the predominant contributors to SVD (Thompson and Hakim, 2009), while minor risk factors include smoking and male sex (Mok and Kim, 2015). Genetic predisposition is another acknowledged contributor to sporadic SVD (Dichgans, 2007).

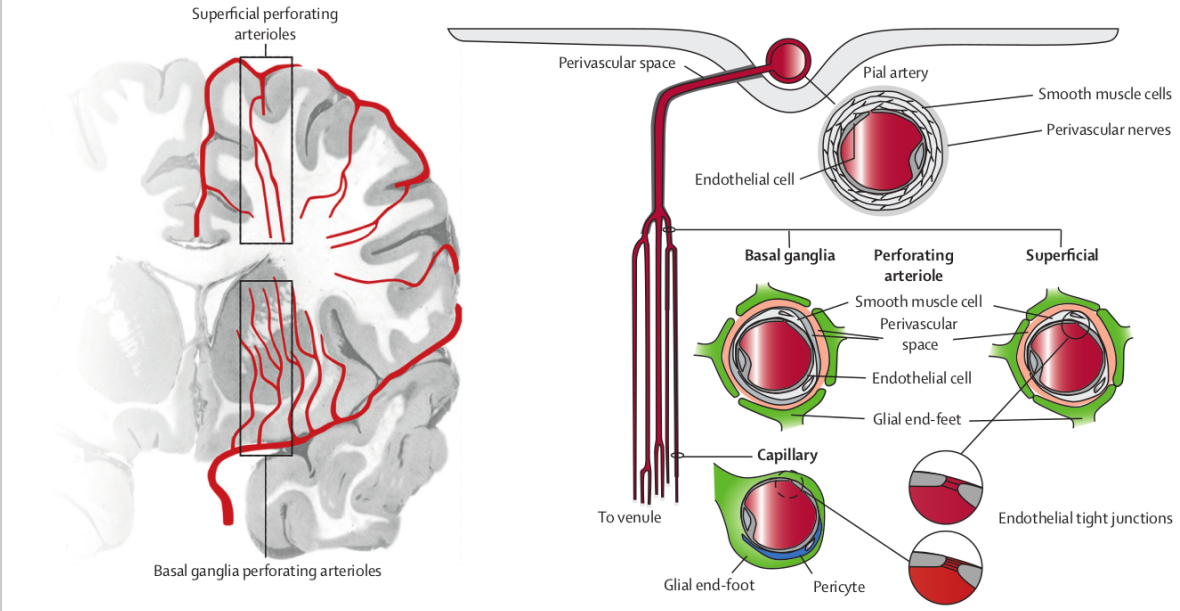

Figure 3.1.: Perforating cerebral arteries and arterioles

Illustration of the macro- (left) and microanatomy (right) of perforating cerebral arteries. While VSMC are found in arteries and arterioles, capillaries are covered by pericytes, instead. Figure from Wardlaw et al. (2013).

Despite a considerable health burden and a growing academic interest, little is known about the pathogenesis, effective prevention and treatment of SVD.

3.1.2 Clinical Features of SVD

Most non-SVD-related strokes are easily recognized due to acute and severe symptoms such as hemiparesis, aphasia or life-threatening circulatory dysfunction. In contrast, SVD-related subcortical infarcts often result in fewer and less noticeable symptoms or even remain clinically silent (Wardlaw et al., 2013).

SVD-related strokes display a favorable early outcome as compared to other stroke types (Jackson and Sudlow, 2005). However, their long-term impact on the daily living functions of patients is considerable, and may, as the disease progresses, almost entirely deprive them

of autonomy (Pantoni, 2010; Mok and Kim, 2015). Indeed, common SVD manifestations include motor and executive slowing (Craggs et al., 2014), dysarthria, urinary incontinence and mood changes up to severe clinical depression as well as progressive dementia.

3.1.3 Neuroimaging in SVD

It is challenging to visualize small vessels *in vivo* (Wardlaw et al., 2001). Hence, SVD is typically defined by the presence of characteristic lesions detected by magnetic resonance imaging (MRI) or computed tomography (CT) (Haffner et al., 2016). A hallmark finding are so-called *lacunar infarcts* (Figure 3.2a), which result from occlusion of perforating small arteries (as depicted in Figure 3.1). Therefore, they are seldom found in the cortex, but much rather in the white and deep gray matter (Rincon and Wright, 2014). Lacunar infarcts have a diameter of up to 20 mm (Wardlaw et al., 2009) and may take one of three possible courses of development. First, some lacunar infarcts result in the formation of *lacunes* (Figure 3.2b), which are trabeculated cavities filled with cerebrospinal fluid (CSF). Second, lesions may gradually dissipate in MRI, making it difficult to meaningfully estimate true lacunar infarct burden in a patient (Potter et al., 2010). A third possible outcome is the formation of white matter hyperintensities (WMH) (Figure 3.2c), which are broadly assumed to result from chronic cerebral hypoperfusion (Duering et al., 2013). Further typical neuroimaging findings in SVD include visible perivascular spaces as well as cerebral microbleeds (CMBs) (Staals et al., 2014; Potter et al., 2013).

3.1.4 Histopathology of SVD

From a histopathological point of view, SVD is characterized by a panel of changes to the composition - and ultimately the function - of the vessel wall of small arteries and arterioles. Combined, these changes result in a stenosis and/or loss of elasticity of small vessels, impeding vascular autoregulation and blood flow. Thus, characteristic brain areas supplied by penetrating end-arteries develop typical lesions (see Section 3.1.3) as a result of acute or chronic oxygen and nutrient deprivation (Craggs et al., 2014).

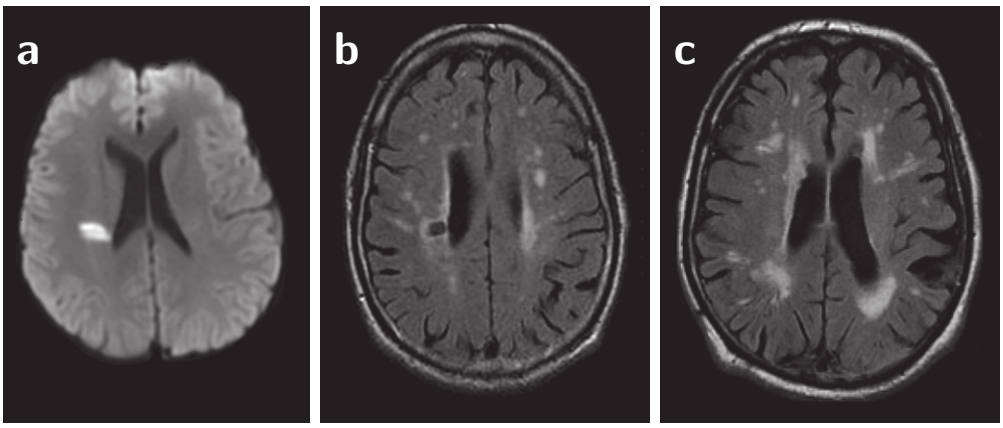

Figure 3.2.: Neuroimaging findings in SVD

(**a**) Acute lacunar infarct (diffusion-weighted MRI). (**b**) CSF-filled cavity formed by a lacunar infarct (fluid-attenuated inversion recovery (FLAIR) MRI). (**c**) WMH (seen as hyperintense areas; FLAIR MRI). Figures from Wardlaw et al. (2013).

One very widespread and prominent histopathological finding in SVD is a progressive hyalinization and fibrosis of vessels with accumulation of ECM components such as fibronectin and collagens (Craggs et al. (2014); see Figure 3.3a-f). This is accompanied by a marked thickening of the tunica intima, while the tunica media is more prone to degeneration or fibrinoid necrosis, potentially resulting in a splitting of the vessel wall referred to as *double barrel* appearance (Pantoni, 2010). A loss of VSMC in the media is also frequently reported (Pantoni, 2010; Thompson and Hakim, 2009). It should be noted, however, that this mostly relies on the analysis of VSMC-specific contraction markers such as α-SMA (see Figure 3.3g-i), rather than medial cell quantification.

While many commonly observed pathological features are shared between sporadic and hereditary SVD, some inherited disorders may present with additional, unique histological findings (Table 3.1).

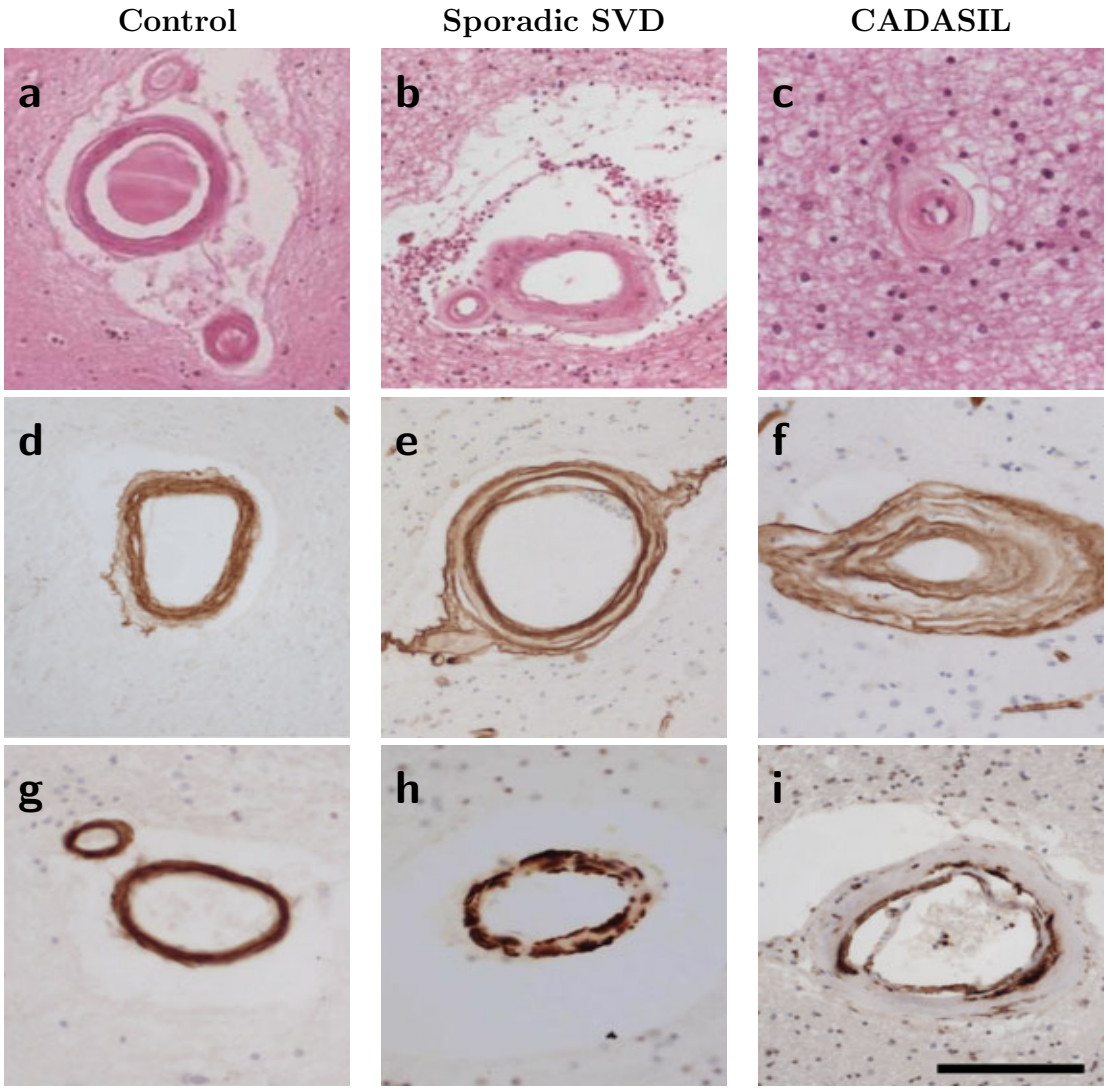

Figure 3.3.: Histopathological hallmarks of SVD

(**a**)-(**c**) H&E staining showing sclerosis, i.e. luminal narrowing and thickening of the vessel wall in sporadic SVD as well as in CADASIL. (**d**)-(**f**) Staining for collagen IV, an extracellular matrix (ECM) component. Increased deposition of collagen IV indicates fibrosis. (**g**)-(**i**) α-smooth muscle actin (α-SMA) staining showing a loss of contractile cells or contractile protein in sporadic and hereditary SVD. Scale bar in (**i**) represents 70 µm in (**c**), 100 µm in (**i**), and 150 µm in all other figures. Figures from Craggs et al. (2014).

3.1.5 Hereditary SVD

Besides sporadic SVD, some monogenic forms, including CADASIL, the most common form of inherited SVD, exist. Representative examples are provided in Table 3.1. These inherited disorders are rather rare, but provide useful models for the identification of basic SVD mechanisms.

Indeed, although the pathomechanisms underlying distinct monogenic SVDs obviously differ, there is increasing evidence for convergent pathways:

(i) Recent work has identified alterations of the cerebrovascular matrisome, i.e. the entirety of proteins either constitutive or associated with the extracellular matrix, in cerebral autosomal-dominant/-recessive arteriopathies with subcortical infarcts and leukoencephalopathy (CADASIL/CARASIL) and *COL4A1/-2*-related SVD (Joutel and Faraci, 2014; Zellner et al., 2018)

(ii) The expression and/or location of TGF-β signaling pathway components was reported to be altered in both CADASIL and CARASIL (Monet-Leprêtre et al., 2013; Kast et al., 2014; Beaufort et al., 2014)

(iii) The CARASIL-relevant protein HTRA1 was found to accumulate in CADASIL brain vessels (Monet-Leprêtre et al., 2013; Zellner et al., 2018)

In addition, features initially described in familial SVD cases have also been identified in the more frequent sporadic forms. A remarkable example is provided by the work of Duering et al., reporting that lesions within neuronal circuits typically associated with SVD contribute to progressive vascular cognitive impairment, not only in CADASIL (Duering et al., 2011), but also in sporadic SVD (Duering et al., 2014).

	CADASIL	CARASIL	RVCL	Anderson-Fabry disease (AFD)	*COL4A1/-2*-related SVD
Causative gene(s)	*NOTCH3*[A]	*HTRA1*[F]	*TREX1*[J]	*GLA*[M]	*COL4A1*; *COL4A2*
Mode of inheritance	autosomal dominant[B]	autosomal recessive[F]	autosomal dominant[J]	X-linked[J]	autosomal dominant[O]
OMIM[1] catalog number of phenotype(s)	125310	600142	192315	301500	607595; 611773; 614483; 614519
Clinical features					
Cognitive impairment/dementia	yes[C]	yes	yes	rare	no
Mood disturbances/depression	yes[D]	no	yes	no	yes
Migraine	yes (with aura)[C]	no	yes	no	yes
Other	seizures	alopecia, spondylosis[G]	retinopathy, Raynaud's phenomenon	angiokeratoma, renal and cardiac involvement[N]	kidney defects, developmental delay, infantile hemiparesis[O]
Radiological findings					
White matter hyperintensities	yes	yes	yes	yes	yes[K]
Subcortical infarcts	yes	yes	yes	rare	yes
Other	brain atrophy		subcortical pseudotumors[K]	large infarcts (e.g. by cardioembolism)	periventricular cysts, deep intracerebral hemorrhage, retinal pathologies[K]

Vascular pathology	deposits of granular osmiophilic material (GOM) in the vessel wall, thickening of the intima[A]	pathological dilation of vessels, thickening and splitting of the intima	obliteration of capillaries, microaneurysms[L]	accumulation of unprocessed glycosphingolipids[M]	interruption and thickening of basement membrane in small and large vessels alike[O]
Pathomechanism	proposed: extracellular aggregation of the extracellular domain of the Notch3 receptor, pathological recruitment of ECM components within these aggregates[E]	HTRA1 loss of function[F], accumulation of ECM-related HTRA1 substrates[Q], reduced TGF-β signaling[P]	mislocalization of truncated TREX1[J]	loss of function of the lysosomal enzyme α-galactosidase A[M]	fragile and damaged vascular basement membranes caused by dysfunctional type IV collagen α1/α2 chain[L]

Table 3.1.: Features of selected hereditary SVDs. References: **A**: Joutel et al. (1996); **B**: Chabriat et al. (2009); **C**: Dichgans (2002); **D**: Vahedi et al. (2004); **E**: Monet-Leprêtre et al. (2013); **F**: Hara et al. (2009); **G**: Fukutake (2011); **J**: Richards et al. (2007); **K**: Tan and Markus (2015); **L**: Ringelstein et al. (2010); **M**: Zarate and Hopkin (2008); **N**: Mehta et al. (2004); **O**: Lanfranconi and Markus (2010); **P**: Beaufort et al. (2014); **Q**: Zellner et al. (2018)

[1] Online Mendelian Inheritance in Man (OMIM, `http://www.omim.org/`), online catalog of genetic disorders maintained by the Johns Hopkins University (Baltimore, USA)

3.2 The HTRA1 Protease: an Emergent Player in Familial SVD

3.2.1 CARASIL

3.2.1.1 Clinical and Histopathological Manifestations of CARASIL

CARASIL is a rare, recessively inherited form of SVD with typical disease onset occurring at 20 to 30 years of age. It was first described by Maeda et al. (1976) as a "Familial unusual encephalopathy of Binswanger's type without hypertension" in a small number of Japanese families. More recently, patients have been identified throughout mainland Asia (China, India, Pakistan) as well as across Europe (e.g., Spain, Romania, Portugal, France) (Menezes Cordeiro et al., 2015; Chen et al., 2013; Diwan et al., 2012).

CARASIL shares many clinical and pathological features with other SVDs. Specifically, it is characterized by early-onset WMHs (Figure 3.4a), lacunar infarcts and progressive dementia (Fukutake, 2011). In addition, patients often suffer from extraneurological symptoms such as vertebral disc herniation, spondylosis deformans (Figure 3.4b) and alopecia (Figure 3.4c).

On a histopathological level, CARASIL is characterized by vascular degeneration selectively affecting the small cerebral arteries. Patient arterioles display a pathological dilation (Oide et al., 2008), accompanied by a thickening of the intima (the general architecture of a vessel is depicted in Figure 3.6), a thinning of the media with accumulation of hyaline material and splitting of the internal elastic lamina. Moreover, immunohistochemistry revealed a drastic loss of the smooth muscle cell marker α-SMA (Figure 3.4d). This reduction has been predominantly attributed to VSMC loss (Arima et al., 2003; Oide et al., 2008), however it might reflect an altered VSMC phenotype (see Section 3.3), as proposed by Ikawati et al. (2018) and evaluated over the course of my doctoral thesis (see Section 3.4 and Chapter 5).

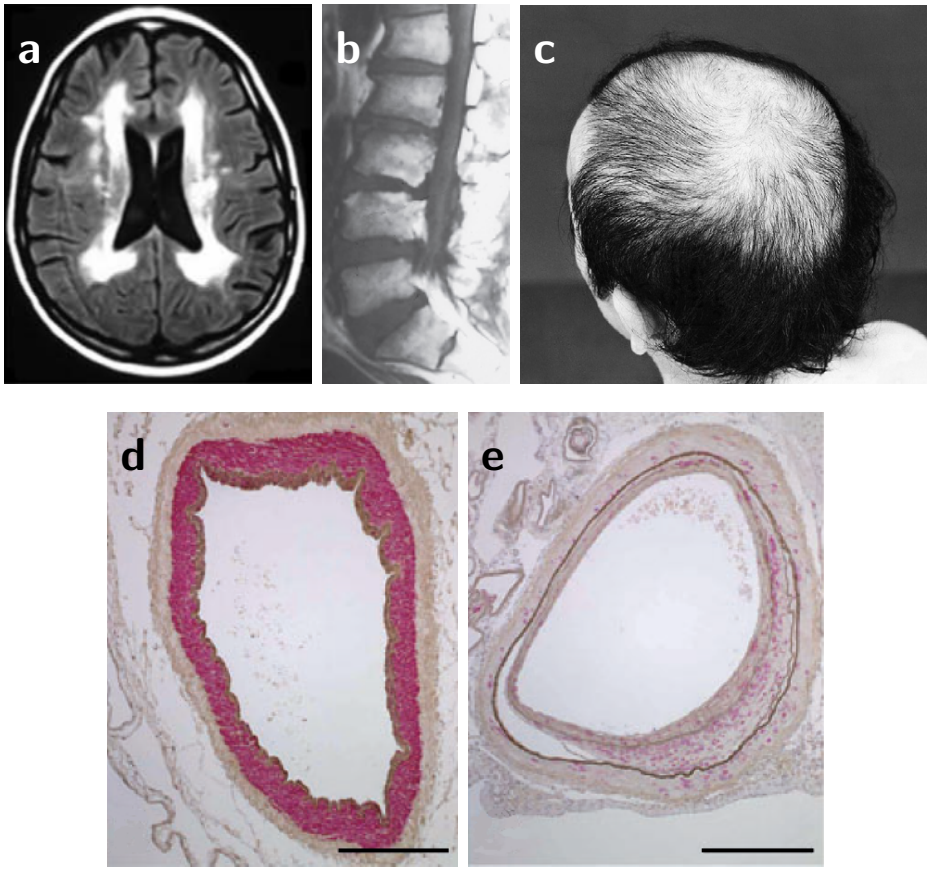

Figure 3.4.: Hallmarks of CARASIL

(**a**) Diffuse leukoencephalopathy with WMH (FLAIR MRI). (**b**) Lumbar spondylosis (MRI). (**c**) Alopecia. (**d**) and (**e**) Weigert and α-SMA (dark red) double staining in leptomeningeal arteries from a control individual (left) and a CARASIL patient (right). Scale bars indicate 500 µm. Figure (a) from Fukutake (2011), (b) reproduced with permission from Hara et al. (2009) (Copyright Massachusetts Medical Society), (c) Menezes Cordeiro et al. (2015), (d) Oide et al. (2008).

3.2.1.2 Molecular Pathomechanisms in CARASIL

In 2009, a genome-wide linkage analysis in CARASIL families led to the identification of *HTRA1* (high temperature requirement A1) as causative gene for the disorder (Hara et al., 2009).

HTRA1 is a ubiquitously expressed, secreted serine protease involved in cell signaling, differentiation and survival. Although CARASIL provides the strongest evidence for a causative role of HTRA1 in human disease, the protein HTRA1 has been shown to be aberrantly expressed in an increasing number of disorders (as reviewed in Clausen et al. (2011)):

(i) Single nucleotide polymorphisms (SNPs) in the HTRA1 promoter region are associated with a predisposition for age-related macular degeneration

(ii) HTRA1 is overexpressed in and suspected to contribute to e.g., arthritis and preeclampsia

(iii) HTRA1 is repressed during malignant transformation and acquisition of chemoresistance

In mid-2017, a total of 16 different pathogenic HTRA1 mutations had been identified in CARASIL cases. These include one intronic mutation affecting messenger RNA (mRNA) splicing (Menezes Cordeiro et al., 2015) and various missense or nonsense mutations, targeting all *HTRA1* exons (Roeben et al., 2016). The majority of mutations was investigated and found to impair HTRA1 expression and/or protease activity. This suggests that lack of processing of HTRA1 substrates is a crucial pathomechanism in CARASIL.

HTRA1 targets a number of substrates including ECM proteins and growth factors. Particularly, my host laboratory recently identified the TGF-β binding partner latent TGF-β binding protein (LTBP)-1 as a novel substrate of HTRA1, and proposed that HTRA1-dependent cleavage of LTBP-1 facilitates TGF-β signaling (see Section 3.2.1.3 and Figure 3.5). Accordingly, a strong reduction of TGF-β signaling was observed in fibrob-

lasts and brain tissue from *HTRA1*$^{-/-}$ mice as well as in skin fibroblasts from one CARASIL patient (Beaufort et al., 2014).

TGF-β is further introduced in the next sections, as I examined the status of TGF-β signaling in CARASIL (see Section 3.4 and Chapter 5) over the course of my thesis.

3.2.1.3 TGF-β Signalopathy in CARASIL and Other Vascular Disorders

TGF-β and TGF-β signaling

The transforming growth factor-β isoforms (TGF-β1, -2 and -3) form a protein superfamily together with growth differentiation factors and bone morphogenic proteins (BMPs) (Gaarenstroom and Hill, 2014). TGF-β is co-expressed and co-secreted as a covalent complex together with its binding partner LTBP-1. Upon secretion, LTBP-1 anchors the inactive complex to ECM components such as fibrillins and fibronectin (Hynes, 2009). TGF-β activation involves its proteolytic processing or a conformational change induced by interactions between cell membrane receptors of the integrin superfamily and the ECM. As previously stated, my host laboratory recently evidenced a role of HTRA1 in TGF-β activation, involving the cleavage of LTBP-1 and the release of the LTBP-1/TGF-β complex from the ECM (Beaufort et al., 2014) (see Section 3.2.1.2 and Figure 3.5).

At the surface of the target cell, active TGF-β binds to TGF-β-receptor 1 (TGFBR1), resulting in the recruitment of TGFBR2, and ultimately in the phosphorylation of these serine/threonine-specific receptor kinases (Vizan et al., 2013). The activated receptor complex then phosphorylates intracellular mediators from the *mothers against decapentaplegic homolog (Smad)* protein family (Schnaper et al., 2002). The so-called receptor-regulated SMADs (R-SMADs) 2 and 3 associate with the only member of the common-mediator SMAD (co-SMAD) subfamily, Smad4, and translocate into the nucleus (Massagué, 2012).

There, Smad complexes interact either with DNA-binding transcription factors or directly bind to SMAD-binding elements (SBEs), promoting the transcription of target genes (Mullen et al., 2011) (Figure 3.5). These include connective tissue growth factor (CTGF) and plasminogen activator inhibitor-1 (PAI-1), which are widely used as surrogate mar-

kers for TGF-β signaling activity (Massagué, 2012; Dennler et al., 1998). Furthermore, many proteins either directly involved in cell contraction (e.g., α-SMA, SM-MHC, SM22, calponin) or associated with the contractile VSMC phenotype (e.g., myocardin, integrins) are regulated by TGF-β (Rensen et al., 2007; Assinder et al., 2009; Miano, 2015) (see Section 3.3).

TGF-β signalopathy in vascular disorders

TGF-β signaling is proposed to be strongly reduced under HTRA1-deficient conditions and in CARASIL (Beaufort et al., 2014). More generally, TGF-β is well-known to be involved in a variety of vascular disorders. For instance, mutations in either Smad, TGF-β, TGFBR or the LTBP-1 binding partner fibrillin are well-established as a cause for Marfan's and Loeys-Dietz syndrome (MacCarrick et al., 2014).

TGF-β expression and/or activity is also deregulated in and suspected to contribute to vascular diseases including atherosclerosis (Pardali, 2012) and CADASIL (see Section 3.1.5). In good agreement with those observations, animal models either deficient for or overexpressing TGF-β pathway components display a severe vascular phenotype (Ishtiaq Ahmed et al., 2014).

3.2.2 *HTRA1*-related Late-onset SVD

CARASIL patients all bear homo- or compound heterozygous mutations. Although detailed clinical examination of heterozygous parents of CARASIL patients had revealed that some exhibit mild SVD manifestations (Bianchi et al., 2014), HTRA1 mutations have been considered to be strictly recessive until recently. Indeed, in 2015, as I had started my experimental work, Verdura et al. (2015) identified heterozygous *HTRA1* mutations as a major cause of autosomal dominant SVD, using whole exome sequencing in a family with autosomal dominant SVD and subsequent genotyping of 201 unrelated probands with familial dominant SVD. This was further confirmed in an independent patient sample (Nozaki et al., 2016) as well as in single cases (Bayrakli et al., 2014; Bougea et al., 2017).

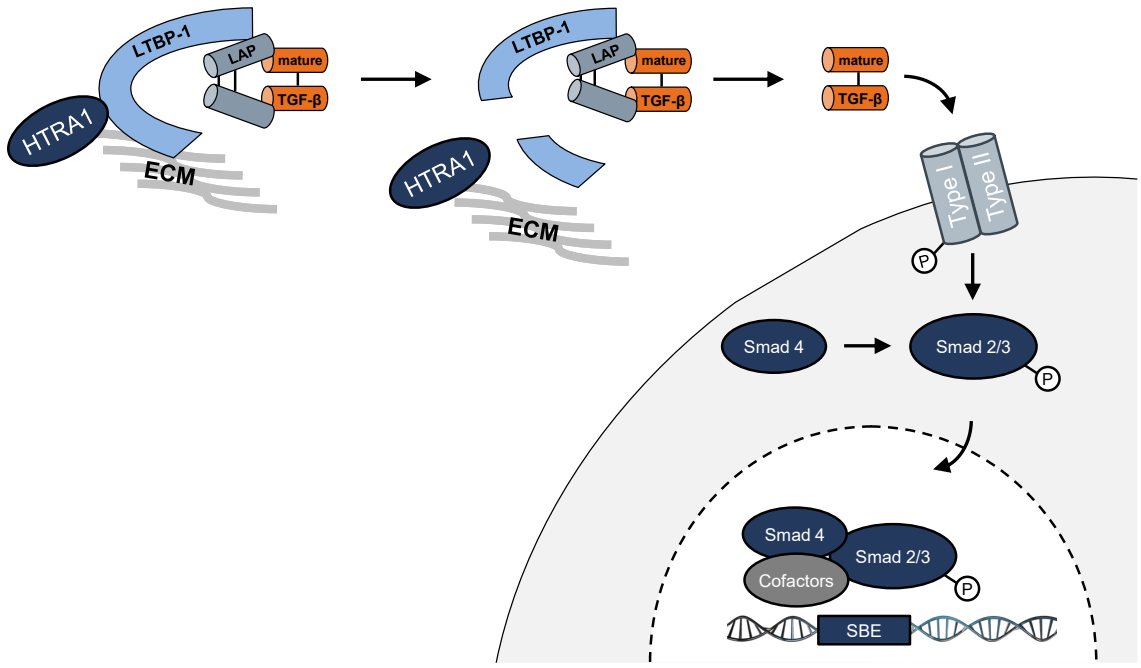

Figure 3.5.: HTRA1 facilitates TGF-β signaling

HTRA1 cleaves LTBP-1 and releases the LTBP-1-TGF-β-complex from the ECM. Subsequently, mature TGF-β binds to the TGFBR1 which then forms a complex with TGFBR2 to phosphorylate and release either Smad2 or -3. Next, the R-SMAD conjugates with Smad4 and migrates into the nucleus, where it associates with one or more transcriptional co-factors at the SMAD-binding element (SBE) to initiate the expression of target genes.

The amino acid residues targeted by heterozygous HTRA1 mutations partly overlap with those involved in CARASIL and most mutations disrupt HTRA1 protease activity. While all patients display WMHs, their clinical features range from cognitive decline to stroke and largely differ from those observed in CARASIL cases by a much later symptom onset (50 - 70 years of age) and by the absence of extraneurological symptoms.

Notably, the distinguishing features between CARASIL-related "recessive" mutations and "dominant" mutations as well as the mechanisms underlying the pathogenicity of the heterozygous mutations are unclear. These mechanisms might involve e.g., haploinsufficiency or dominant-negative effects (Verdura et al., 2015; Uemura et al., 2019).

3.3 Vascular Smooth Muscle Cell (VSMC) Phenotypic Switching

3.3.1 Location of VSMC

Based on their diameter and architecture, cerebral vessels are commonly classified as arteries (with diameters $> 100\,\mu m$), arterioles (with diameters ranging between $100 - 10\,\mu m$) and capillaries (with diameters of $10 - 5\,\mu m$) (Bentov and Reed, 2015).

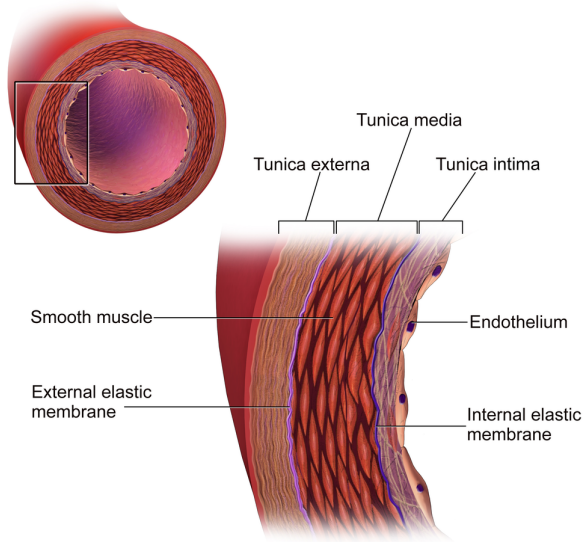

Figure 3.6.: Composition and layers of the arterial wall

Section of an artery. See also Figure 3.1 for illustrations of arterioles and capillaries. Figure from `Blausen.com` staff at Wikimedia Commons.

Arteries and arterioles are subjected to high blood pressure. Their vascular wall is organized in three layers (as illustrated in Figure 3.6). The innermost of these, the *tunica intima*, consists of the internal elastic lamina and endothelial cells. Adjacent to it, the *tunica media* harbors the vast majority of VSMC and varying amounts of elastic tissue, depending on the size of the artery. The outermost layer, the so-called *tunica adventitia*, is separated from the *tunica media* by the external elastic lamina and contains collagen-rich connective tissue and fibroblasts (Kohn et al., 2015).

In contrast, capillaries are subjected to lower blood pressure. They are devoid of elastic laminae as well as VSMC, and their endothelium is covered by a single layer of pericytes (Bentov and Reed, 2015).

3.3.2 Anatomy and Function of VSMC

VSMC are fusiform cells located mainly in the tunica media of arteries, arterioles, veins and venules. In contrast to skeletal muscle cells, they are mononuclear.

Mature VSMC display a so-called *contractile* phenotype. They express a panel of proteins including α-SMA, smooth muscle protein 22-α / transgelin (SM22), calponin and smooth muscle myosin heavy chain / myosin-11x (SM-MHC) that is directly involved in cell contraction and/or in cell-cell or cell-ECM interaction, such as integrins and cadherins (Table 3.2) (Iyemere et al., 2006). The contractile cell phenotype is further characterized by a low proliferation rate and minimal migratory activity.

VSMC are major regulators of the vascular tone and diameter and thus ultimately of blood pressure, flow and distribution (Gomez and Owens, 2012).

3.3.3 VSMC Plasticity in Health and Disease

3.3.3.1 Physiological VSMC plasticity

Contrary to many other cell types, mature VSMC conserve a high degree of plasticity (Owens et al., 2004). For instance, in response to vascular injury, VSMC downregulate the expression of contractile proteins, increase their proliferation and migration rates and/or up-regulate the expression of ECM components such as type I collagen and fibronectin (Rensen et al., 2007) to acquire a so-called *proliferative* and/or *synthetic* phenotype (Figure 3.7; Table 3.2). This process is commonly referred to as *phenotypic switching* and is a major contributor to wound healing.

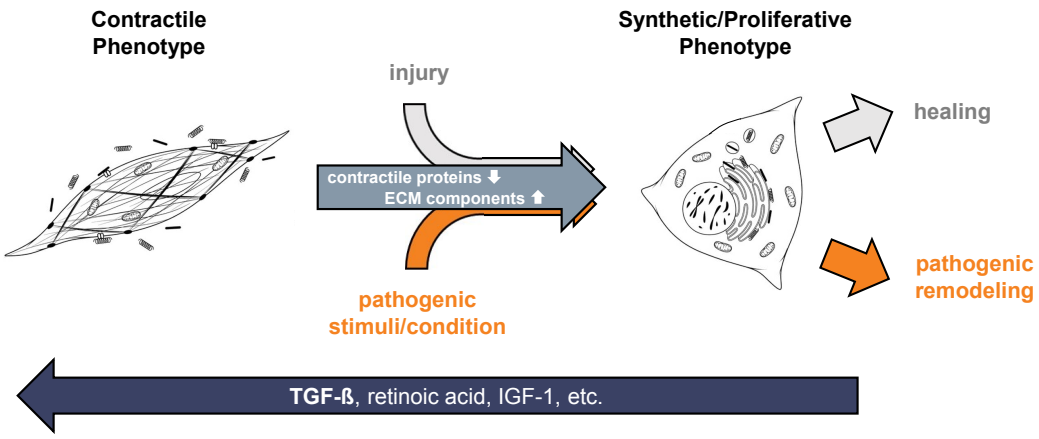

Figure 3.7.: Regulation of VSMC phenotypic switching

While being an important repair and healing mechanism, VSMC phenotypic switching has been shown to be inducible by stimuli such as atherosclerosis or genetic conditions, resulting in pathogenic remodelling. As depicted here, the best-described phenotypes for VSMC are the contractile (left) and synthetic/proliferative phenotype with increased migratory activity (right). Physiologically, contractile VSMC switching is counterbalanced by signal transducers such as TGF-β, retinoids, and insulin-like growth factor (IGF)-1.

3.3.3.2 Pathological VSMC Phenotypic Switching

While providing a powerful tool for the vasculature to react adequately to adverse environmental settings, the high degree of VSMC plasticity also provides the basis for undesirable changes of cell phenotype (Figure 3.7). Triggers for such changes include pathogenic preconditions such as inflammation, chronic disease, inherited disorders, or combinations of the three. The resulting VSMC phenotypic switching may then lead to further acceleration of the causative disease (Owens et al., 2004).

While "phenotypic switching" was originally described as a dichotomous transition between contractile and proliferative/migratory cell specialization, its understanding has meanwhile transitioned from de-differentiation to a broader spectrum of changes that may gradually develop. Notably, VSMC have been increasingly shown to express markers typically associated with other cell types and functions such as phagocytic and osteogenic cells (see Table 3.2).

	Contractile	Proliferative/Synthetic	Phagocytic	Calcifying
	α-SMA	type I collagen	galectin-3	Runx2
	calponin	fibronectin	CD68	Osterix
	SM22			Msx2
	SM-MHC			
	α1/β1 integrin			
	N-/T-cadherin			
Reference(s)	Rensen et al. (2007)	Rensen et al. (2007)	Rosenfeld (2015)	Iyemere et al. (2006)

Table 3.2.: Markers associated with various VSMC phenotypes

Due to its high incidence and extensive health burden, atherosclerosis is the condition where VSMC phenotypic switching has been studied to the greatest extent. As expected, contractile markers such as α-SMA, SM22 and SM-MHC have been shown to be strongly reduced in VSMC within atherosclerotic environments (Gomez et al., 2013). Strikingly,

in addition, markers typically associated with macrophages such as galectin-3[2] and CD68 were found to be markedly up-regulated (Feil et al., 2014; Shankman et al., 2015). Such expression of phagocytosis-related markers in VSMC was shown to be inducible upon loading of cultured VSMC with cholesterol to simulate the milieu of an atherosclerotic lesion, which not only resulted in α-SMA, SM22 and calponin-1 downregulation, but also in significantly increased expression of galectin-3 and CD68 as well as increased phagocytic activity (Rong et al., 2003; Vengrenyuk et al., 2015; Shankman et al., 2015).

VSMC phenotypic switching has been implicated in a number of genetic conditions. For example, altered expression of contractile markers and resulting contractile dysfunction of VSMCs has been observed in Marfan's as well as in Loeys-Dietz syndrome (LDS; OMIM: 609192 and others), the most characteristic symptom of both being aortic aneurysms (Milewicz et al., 2008). In hereditary SVD, loss of contractile markers has been repeatedly reported as well. Specifically, as shown in Figures 3.3i and 3.4e, there is a pronounced loss of the VSMC hallmark protein α-SMA in patient brain vasculature. Yet, a lack of studies further examining VSMC phenotypic switching in hereditary SVD persists, leading us to the initiation of my thesis work.

3.3.4 Regulation of VSMC Phenotype

3.3.4.1 Physical and Biochemical Factors Affecting VSMC Phenotype

VSMC phenotype is controlled by a rather complex and tightly regulated transcriptional program. Under both physiological and pathological circumstances, this program can be influenced by a variety of environmental factors (Figure 3.7), including:

(i) physical parameters such as shear stress, stretch or mechanical trauma as well as the structure and compliance of the vessel (Rensen et al., 2007)

(ii) interactions with ECM components (e.g. type I/IV collagens) and surrounding cells, both involving adhesion receptors (particularly integrins) (Owens et al., 2004)

[2]galectin-3 is sometimes also referred to as *Mac-2*

(iii) a variety of growth factors and their downstream signaling including angiotensin II, IGF-1, TGF-β (see Section 3.2.1.3), Wnt, platelet-derived growth factor (PDGF) and retinoic acid (RA) (Owens et al., 2004; Wang et al., 2015)

(iv) other biochemical agents such as lipids, nitric oxide (NO) and reactive oxygen species (ROS)

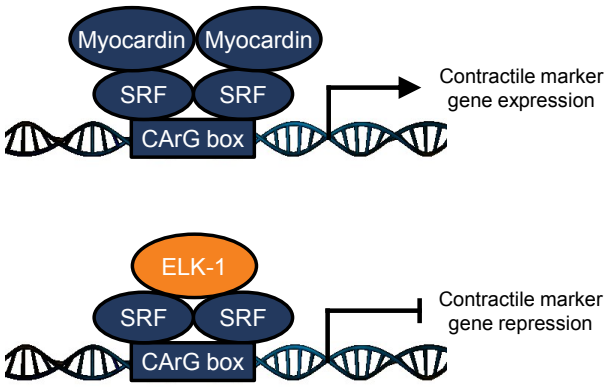

Figure 3.8.: Mechanisms regulating SRF-mediated transcriptional activity

While myocardin promotes serum response factor (SRF)-mediated transcription of CArG-box-containing genes important for VSMC contractile differentiation, Elk-1 may interrupt transcriptional activity via occupation of the myocardin-SRF binding site.

3.3.4.2 Transcriptional Regulation of VSMC Phenotype

The vast majority of contractile phenotype markers such as α-SMA, SM22, SM-MHC, and calponin-1 contain highly conserved regulatory elements within their promoter regions. The three major representatives of such motifs are TGF-β control elements (TCEs), SMAD-binding elements (SBEs) (see Section 3.2.1.3), and serum response elements (SREs), the latter being characterized by the presence of so-called *CArG boxes* (McDonald et al., 2006). CArG boxes are *cis*-elements with a length of 10 base pairs (bp) with the sequence

CC-A/T-GG where "A/T" represents a 6-bp block that is rich in either adenine or thymine or both (Miano, 2003; McDonald et al., 2006). These boxes serve as binding sites for various transcription factors, thus playing a crucial role in the expression of proteins involved in contraction. Often, the promoter regions presented above are located in close proximity to one another. For instance, binding of a transcriptional repressor to a TCE may inhibit transcription from a nearby SRE (Zheng et al., 2010).

Activators of the contractile differentiation program

The CArG box-binding transcription factor SRF is a major contributor to cell differentiation, including that of VSMC. SRF is ubiquitously expressed in a rather stable fashion.

Myocardin is an important co-factor of SRF (Figure 3.8). Its expression is largely restricted to cardiac and vascular smooth muscle tissue (Owens et al., 2004), allowing the SRF/myocardin complex to control gene expression in a cell-specific manner. Myocardin, which is induced by various mediators including TGF-β, is required for VSMC contractile gene expression (Kurpinski et al., 2010). Indeed, low myocardin expression was not only found to correlate with, but also to induce a loss of the contractile phenotype in cells and/or tissues (Miano, 2015). Conversely, overexpression of myocardin induces phenotypic switching towards a contractile phenotype (Long et al., 2008).

Two additional myocardin co-factors (myocardin-like protein (MKL) 1 and 2) have been described[3] (Wang et al., 2002). Like myocardin, their expression is inducible (e.g., by TGF-β) and their down-regulation reduces the expression of contractile proteins, while their overexpression activates the contractile differentiation program (Cen et al., 2004).

Repressors of the contractile differentiation program

The so-called ternary complex factors (TCFs) constitute a group of three transcription factors (Elk-1, -3, and -4) that belong to the ETS-domain containing protein superfamily. TCFs are known to repress cell differentiation and promote cell proliferation in a man-

[3]Other commonly used names for these proteins include *megakaryoblastic leukemia proteins* 1 and 2 as well as *myocardin-related transcription factor (MRTF)-A* and *-B*

ner antagonistic to that of myocardin and the MKLs (Buchwalter et al., 2004; Wang et al., 2004). While the mechanisms of action of the TCFs are not yet fully understood, they include competition of Elk-1 with myocardin and MKLs for a common SRF docking site (Wang et al. (2004); Zhou et al. (2005); Figure 3.8) and initiation of a synthetic/proliferative differentiation program.

A further class of transcriptional modulators of VSMC differentiation is the Krueppel-like factor (Klf) family of zinc-finger-containing transcription factors. Among the 17 Klfs found in humans, Klf4 (also known as *gut-enriched Krueppel-like factor (GKLF)*) and -5 have attracted most attention in a vascular context (Mcconnell and Yang, 2010). Klfs are expressed at very low levels in the normal vessel wall but are markedly induced by e.g., vascular injury (Diakiw et al., 2013; Liu et al., 2003; Yoshida et al., 2008). Klfs repress the VSMC contractile differentiation program, and have been proposed to promote atherosclerosis-related phagocytic VSMC differentiation, a feature recently established for Klf4 (Shankman et al., 2015; Rosenfeld, 2015).

Several mechanisms have been shown to mediate Klf action. Indeed, Klf4 may inhibit SRF binding to the CArG box (Zheng et al., 2010) and antagonize the SRF/myocardin axis. Similarly, Klf5 was found to disrupt the SRF-myocardin transcriptional complex (Zhang et al., 2015). In addition, Klf4 may not only inhibit TGF-β via binding to TCEs (Liu et al., 2003), but also by competing with Smad3 for SBE interaction (Hu et al., 2007).

Alternatively, Klf4 may associate with Elk-1 and histone deacetylase (HDAC)2, resulting in the binding of the complex to G/C-rich repressor elements within contractile VSMC gene promoter regions (Salmon et al. (2012); see Figure 3.9).

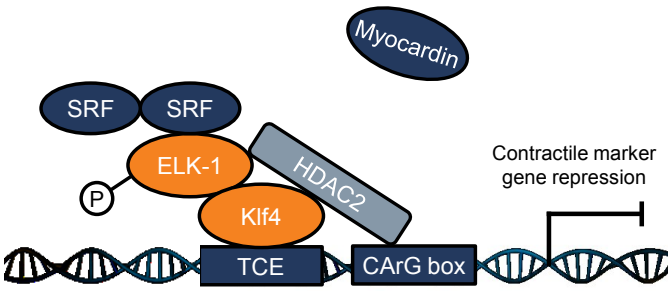

Figure 3.9.: Klf4 suppresses contractile marker transcription

Klf4 may aggregate with phosphorylated Elk-1 and HDAC2, resulting in suppression of contractile marker genes through several mechanisms of action. These include competition for SRF binding sites with myocardin, direct occupation of TCEs within VSMC gene promoter regions as well as indirect blockade of the CArG box within SREs through chromatin compaction.

3.4 Aim of the Thesis

TGF-β signaling plays a major role in the regulation of contractile cell differentiation. Based on the analysis of *HTRA1*$^{-/-}$ mouse brain tissue and cells and of skin fibroblasts from one CARASIL patient, my host laboratory linked the hereditary cerebral small vessel disease CARASIL to a drastic reduction of TGF-β signaling (Beaufort et al., 2014). Notably and although heterozygous *HTRA1* mutations have recently been identified as a cause of late-onset SVD (Verdura et al., 2015; Nozaki et al., 2016), the status of TGF-β signaling in this condition has not been examined yet.

On a different note, a reduction of VSMC contractile markers such as α-SMA has been observed in cerebral vessels of CARASIL and CADASIL patients (Oide et al., 2008). While this finding was attributed to cell loss, it might rather reflect cell phenotypic switching, a process well-described in wound healing and atherosclerosis, that has attracted considerable attention as an emerging pathomechanism in vascular diseases.

Based on these observations, it was hypothesized that in CARASIL (or late-onset HTRA1-related SVD), reduced TGF-β signaling activity might result in VSMC phenotypic switching towards a less contractile state, a process likely to contribute to vascular dysfunction.

Therefore, the aims of my project were:

(i) To evaluate the impact of heterozygous *HTRA1* mutations on TGF-β signaling;

(ii) To characterize the phenotype of cells bearing hetero- or homozygous *HTRA1* mutations both regarding contractile protein expression and cell function;

(iii) To explore strategies to restore the cell phenotype.

HTRA1-related SVDs are rare disorders and access to patient material is challenging. I thus selected human primary skin fibroblasts available in the laboratory as a model for

my investigations. Notably, skin fibroblasts express a large panel of contraction markers overlapping with those expressed by VSMC and are able to contract.

Additionally, to allow for *in situ* analysis of cerebral blood vessels, I extended my investigations to *HTRA1*$^{+/+}$ or $^{-/-}$ mice.

4 Material and Methods

4.1 Cell-based Experiments

4.1.1 Human Skin Fibroblasts

Primary cultures of human skin fibroblasts from healthy control individuals (n = 6) were kindly provided by the Department of Dermatology of the Ludwig-Maximilians-University (LMU) Munich, E. Tournier-Lasserve (Lariboisière Hospital / Paris Diderot University) and D. Werring and H. Houlden (University College London Hospital). Skin fibroblasts from homo- and heterozygous *HTRA1* mutation carriers (see Table 4.1) were kindly provided by E. Tournier-Lasserve, D. Werring and H. Houlden, and A. Federico (Department of Medicine, Surgery and Neurosciences, University of Siena). The use of these primary cultures has been approved by the ethics committee of the LMU.

4.1.2 Cell Culture Conditions

Skin fibroblast cultures were grown in Dulbecco's modified Eagle's medium (DMEM) / GlutaMAX containing 10 % (v/v) fetal calf serum (FCS), 100 µg/mL streptomycin and 100 U/mL penicillin (all from Invitrogen, Carlsbad, USA). Cultures were maintained in the presence of 5 % CO_2 at 37°C in a humidified chamber (Binder 9040-0038; Binder, Tuttlingen, GER) and were manipulated in a sterile vertical laminar flow hood (Herasafe KS; Thermo Fisher Scientific, Waltham, USA). Absence of *Mycoplasma* was ensured by enzymatic activity assay using the MycoAlert Plus detection kit (Lonza, Basel, SUI). For

Culture referred to as	Zygosity	Mutation(s)	Reference
Het1	heterozygous	c.973-1 G>A / p.Y325-L335del[A]	Verdura et al. (2015)
Het2	heterozygous	c.497G>T / p.R166L[B]	Verdura et al. (2015)
Het3	heterozygous	c.497G>T / p.R166L[B]	Verdura et al. (2015)
Het4	heterozygous	c.126delG / p.E42fs[C]	Bianchi et al. (2014)
Het5	heterozygous	c.961G>A / p.A321T[B]	Bianchi et al. (2014)
Pat1	homozygous	c.517G>A / p.A173T[B]	Khaleeli et al. (2015)
Pat2	compound heterozygous	c.126delG / p.E42fs[C] c.961G>A / p.A321T[B]	Bianchi et al. (2014)
Pat3	compound heterozygous	c.497G>A / p.R166H[B] c.830delA / G276fs[C]	E.Tournier-Lasserve (unpublished)

Table 4.1.: Characteristics of patient skin fibroblast cultures used for this project. **A**: Intronic mutation predicted to affect splicing and resulting in skipping of exon 5. This exon contains the catalytic serine. **B**: Missense mutation targeting HTRA1 protease domain and disrupting its enzymatic activity. **C**: Deletion resulting in a premature interruption of the reading frame. The resulting mutant HTRA1 protein lacks one or more catalytic residues.

passaging, cells were washed with phosphate-buffered saline (PBS), detached with 0.25 % (w/v) trypsin/ethylenediaminetetraacetic acid (EDTA), then seeded (dilution 1 : 3 to 1 : 10) in a new flask containing fresh medium. For all experiments described below, fibroblasts were used at a comparable passage number.

4.1.3 Preparation of Cell Extracts

Unstimulated cells Skin fibroblasts were grown in T75 flasks until a high cell density was achieved. Following a brief rinse with PBS, cells were maintained in 10 mL serum-free DMEM for 72 hours.

TGF-β stimulation High-density cultures of fibroblasts in P6 wells were rinsed with PBS and kept for 72 hours in 1 mL serum-free culture medium with 0.5 or 5 ng/mL mature recombinant human TGF-β (R&D Systems, Minneapolis, USA). For the cell contraction assay (see Section 4.1.4), one volume of serum-free medium containing 10 ng/mL TGF-β was added immediately after gelation. For the viability assay (see Section 4.1.5), one volume of serum-free medium containing 10 ng/mL TGF-β was added to the cell suspension.

Cell lysis All following steps were performed at 4 °C.

For protein analysis, cells were rinsed with PBS, then exposed for 30 minutes to a buffer composed of 10 mM Tris, 100 mM NaCl, 2 mM EDTA, 50 mM NaF, 20 mM $Na_4P_2O_7$, 2 mM Na_3VO_4, 0.5 % (v/v) sodium deoxycholate, 1.5 % (w/v) sodium dodecyl sulfate (SDS), 1 % (v/v) Triton X-100 and 10 % (v/v) glycerol, pH 7.6 with cocktails of phosphatase and protease inhibitors (Roche, Basel, SUI). 100-200 µL were used to lyse the content of P6 wells and 500 µL were used for T75 flasks. Subsequently, debris was removed by centrifugation of the lysates at 11,000 g for 15 minutes.

For mRNA isolation, cells were briefly rinsed with PBS, followed by addition of Buffer RLT (Qiagen, Venlo, NED) with 1 % (v/v) β-mercaptoethanol (500 µL per T75 flask). For homogenization, the QIAshredder kit (Qiagen) was used according to the manufacturer's instructions.

4.1.4 Cell Contraction Assay

10^4 skin fibroblasts were added with 1.5 mg/mL collagen type I (BD Biosciences, Franklin Lakes, USA) in a total volume of 200 µL FCS-free DMEM and were cast in a 48-well plate. A cell-free gel was prepared as negative control. After a 5-minute gelation at 37 °C, one volume of complete culture medium was added and gels were detached from the wells using a sterile needle. Plates were maintained at 5 % CO_2 and 37°C for the indicated time period and then scanned using a Perfection 1640SU flatbed scanner (Epson, Tokyo, JPN). The percentage of the well surface area occupied by gel was determined using the ImageJ (Fiji) software.

4.1.5 Cell Viability Assay

The MTT assay (kit from Sigma-Aldrich, St. Louis, USA) was used to evaluate mitochondrial activity as a surrogate marker of cell viability by detecting the conversion of 3-(4,5-dimethylthiazol-2-yl)-2,5-diphenyltetrazolium bromide (MTT) to the purple-colored formazan. In parallel to the contraction assay (Section 4.1.4), 5000 cells were seeded in 96-well plates. At each time point of gel contraction assessment, cells were washed with PBS and exposed to 50 µL of MTT (diluted in serum-free medium to 5 mg/mL) for two hours at 37°C. 50 µL of dimethyl sulfoxide (DMSO) were added and plates were shaken 5 minutes at room temperature (RT) to solve formazan crystals. The optical density (OD) at 560 nm was measured using a Multiskan photometer (Thermo Labsystems) and the corresponding Ascent Software for Multiskan (v2.6; Thermo Labsystems).

4.2 Mouse-based Experiments

4.2.1 Mouse Strains

HTRA1$^{-/-}$ mice, generated by gene trapping (strain HTRA1$^{\mathrm{GT(OST394864)Lex}}$; Taconic, Hudson, USA) were crossed with *C57BL/6* mice (*HTRA1*$^{+/+}$; Charles River, Wilmington, MA,

USA). Animals were kept at the Institute facility under standard conditions and had access to food (ssniff and LASvendi, both Soest, GER) and water *ad libitum*. Animal care and breeding as well as tissue harvest were performed in accordance to the German Animal Welfare Law and in compliance with the Government of Upper Bavaria.

4.2.2 Genotyping

Genotyping was performed before and after animal sacrifice using ear and tail biopsies, respectively. DNA was extracted by incubation of 1-mm-long tissue pieces with 100 µL of 50 mM NaOH for 30 minutes at 97° C. Afterwards, 30 µL of 1 M tris(hydroxymethyl)aminomethane (Tris)-HCl, pH 7 were added for neutralization. For polymerase chain reaction (PCR), each sample contained Taq Buffer (75 mM Tris-HCl, 20 mM ammonium sulfate, 0.01 % (v/v) Tween 20), 3.25 mM $MgCl_2$, 0.2 mM deoxynucleoside triphosphates (dNTPs), 0.2 mM forward and reverse primers (see below), 2.5 U Taq polymerase and 3 µL tissue lysate in a final volume of 50 µL double-distilled water (ddH_2O). Taq Buffer and polymerase were purchased from Thermo Fisher Scientific. A DNA-free control was included. The primers used were a forward (5'-AGGGTCTCAAGTATCCAGGTTG-3') and a reverse (5'-CCAGAAATAAGACTCGGACTCA-3') primer targeting the wild type (WT) *HTRA1* locus and a reverse primer (5'-ATAAACCCTCTTGCAGTTGCATC-3') detecting the long terminal repeat (LTR) of the gene trapping cassette found in *HTRA1*$^{-/-}$ and $^{+/-}$ mice. A representative example is depicted in Figure A.1, Appendix.

Following a 10-minute initiation step at 95° C, the PCR consisted of 30 cycles, each composed of a 2-minute denaturation period at 95° C, a 1-minute annealing step at 67° C and 30 seconds at 72° C for elongation. After the last cycle, a 10-minute final elongation step at 72° C concluded the run.

PCR amplicons were analyzed using a QiAxcel capillary electrophoresis system with the corresponding QIAxcel DNA Screening Gel Cartridge (both Qiagen).

4.2.3 Brain Harvest

Mice underwent general anaesthesia by intraperitoneal injection of 150 mg/kg Ketamine and 10 mg/kg Xylazine in NaCl 0.9 % (w/v). An incision was made into the liver and, using a needle inserted into the left ventricle of the heart, animals were perfused with 20 mL of PBS.

A neck-to-nose skin incision was made to expose the skull. Scissors were first introduced into the foramen magnum to apply lateral cuts into the cranium and next placed into the frontal fontanelle, twisted by 90° and spread to force open the skull. Subsequently, the brain was extracted, immediately frozen on dry ice and stored at -80° C for later use.

4.2.4 Brain Tissue Lysis

All following steps were performed at 4 °C. Brain tissue was placed in a 2 mL Eppendorf tube and added with 10 µL/mg of buffer containing 50 mM Tris-HCl, 150 mM NaCl, pH 7.4 and cocktails of protease and phosphatase inhibitors at the dilution recommended by the manufacturer (Roche). Metal beads with a diameter of 5 mm (Qiagen) were added and tissue was homogenized at 50 Hz for 3 minutes in a TissueLyser LT bead mill (Qiagen). 1 % (v/v) NP40 and 0.5 % (w/v) SDS were added to the homogenate for 5 minutes and samples were centrifuged at 11,000 g for 30 minutes to remove debris.

4.3 Western Blot (WB)

4.3.1 Protein Concentration Measurement

Total protein concentration was measured via bicinchoninic acid (BCA) assay using the Pierce BCA assay kit (Thermo Fisher Scientific). Samples and bovine serum albumin (BSA) standards in the range of 0.125 to 2 mg/mL were prepared in duplicate. Following a 15-minute incubation period at 37° C, colorimetric analysis at 560 nm was conducted in a Multiskan photometer (specifications see Section 4.1.5).

Substance	Composition
concentration gel	acrylamide 4 % (acrylamide stock: 30 % (w/v) acrylamide and 0.8 % (w/v) N,N'-Methylenebisacrylamide; National Diagnostics, Atlanta, USA), Tris-base 25 mM, SDS 0.08 % (w/v), pH 6.8
migration gel	acrylamide 7.5 – 12.5 %, Tris-base 375 mM, SDS 0.08 % (w/v), pH 8.8
Laemmli buffer	Tris-base 75 mM, glycerol 6 % (v/v), SDS 1.2 % (w/v), DTT 100 mM, bromophenol blue 0.006 % (w/v), pH 6.8
running buffer	Tris-base 25 mM, glycine 192 mM, SDS 0.1 % (w/v), ddH_2O
transfer buffer	Tris-base 25 mM, glycine 192 mM, methanol 20 % (v/v), ddH_2O
TBS-T	Tris-base 10 mM, NaCl 150 mM, Tween 20 0.5 % (v/v) , ddH_2O, pH 8

Table 4.2.: Composition (final concentration) of gels, buffers and solutions used for Western blot.

4.3.2 SDS-PAGE

The composition of the gels and buffers is detailed in Table 4.2. Polyacrylamide gels were prepared in a casting system from Bio-Rad Laboratories (Hercules, USA). Polymerization was induced by addition of tetramethylethylenediamine (TEMED) and ammonium persulfate. Proteins (2-10 µg per lane for cell extracts and 25-50 µg for tissue lysates) were added with Laemmli buffer and heated for 5 minutes at 95° C. Precision Plus Protein All Blue Standard (Bio-Rad Laboratories) was included in each run. SDS-PAGE was performed in a Mini-Protean Tetra Cell apparatus (Bio-Rad Laboratories) filled with running buffer (see Table 4.2) at 150 V for 60 to 90 minutes.

4.3.3 Immunoblot

Proteins were transferred from the gel onto an Immobilon-P polyvinylidene fluoride (PVDF) membrane (Merck Millipore, Billerica, USA) in a Mini-Protean Tetra Cell wet transfer system (Bio-Rad) filled with transfer buffer (see Table 4.2) at 100 V for 45 minutes. Afterwards, membranes were blocked in 4 % (w/v) skim milk powder in TBS-T (see Table 4.2)

for 30 minutes at RT to prevent non-specific antibody binding.

Subsequently, membranes were incubated over night at 4 °C with the primary antibody diluted in blocking solution as stated in Table 4.3. Following three 10-minute washes in TBS-T, the membranes were incubated with a horseradish peroxidase (HRP)-coupled secondary antibody for at least one hour at RT, followed by washings as described above. Alternatively, for mouse brain lysate analysis using mouse primary antibodies, HRP-coupled protein A (dilution 1 : 5000; Sigma-Aldrich) was used to avoid detection of tissue-derived immunoglobulins.

For signal detection, Immobilon Western Chemiluminescent HRP Substrate (Merck Millipore) was dispersed across the membrane which was then inserted into the detection chamber of a Fusion FX7 (with Fusion user interface v15.18; both Vilber Lourmat, Marne-la-Vallée, FRA). Signal quantification was performed using the ImageJ (Fiji) software. Signal obtained from β-actin or tubulin immunoblot was used as a normalizer.

4.4 Immunohistochemistry (IHC)

4.4.1 Section Preparation and Staining

10-µm mouse brain sections were prepared with a CM 1950 cryostat (Leica Microsystems, Wetzlar, GER) and stored at -80° C. To fix tissue, sections were incubated with 4 % (w/v) paraformaldehyde (PFA) for 20 minutes at RT and then permeabilized with 0.1 % (v/v) Triton X-100 in PBS for 20 minutes at RT; each of these steps followed by a short dip in PBS. Blocking of non-specific antibody binding sites was achieved through a subsequent 30-minute incubation step with 5 % (w/v) BSA in PBS. The anti-calponin antibody (diluted in PBS with 0.2 % (w/v) BSA; see Table 4.4) was applied over night at 4° C. After three 5-minute washings in PBS, the sections were incubated for one hour at RT in PBS/BSA with the fluorophore-coupled secondary antibody (corresponding to anti-calponin primary antibody), Cy3-conjugated α-SMA antibody (see Table 4.4), and 4',6-diamidino-2-phenylindole (DAPI; 1.25 µg/mL; Invitrogen). As control, either the anti-

Target antigen	Predicted molecular mass (kDa)	Host	Dilution	Manufacturer
Primary antibodies				
α-SMA	42	mouse	1 : 1 000	Sigma-Aldrich
β-actin	42	rabbit	1 : 500	Sigma-Aldrich
calponin-1	34	rabbit	1 : 1 000	Merck Millipore, Billerica, USA
connexin 43	43	rabbit	1 : 5 000	Abcam, Cambridge, UK
CTGF	38	goat	1 : 2 000	Santa Cruz Biotechnology, Texas, USA
fibronectin	250	mouse	1 : 2 000	Sigma-Aldrich
fibronectin	250	rabbit	1 : 5 000	Sigma-Aldrich
integrin β-1	138	rabbit	1 : 500	Santa Cruz Biotechnology
myocardin	105	mouse	1 : 1 000	R&D Systems, Minneapolis, USA
PDGFR-β	190	goat	1 : 1 000	R&D Systems
phospho-Smad2/3	55 – 60	rabbit	1 : 1 000	Cell Signaling Technologies, Danvers, USA
SM22	22	goat	1 : 1 000	Abcam
Smad2	60	goat	1 : 1 000	Santa Cruz Biotechnology
SM-MHC	220	mouse	1 : 1 000	Merck Millipore
tubulin	50	mouse	1 : 1 000	Sigma-Aldrich
HRP-coupled secondary antibodies				
rabbit immunoglobulin		goat	1 : 10 000	Dako
goat immunoglobulin		rabbit	1 : 10 000	Dako
mouse immunoglobulin		goat	1 : 10 000	Dako

Table 4.3.: Western blot antibodies. A test run was conducted with each antibody to ensure detection of a single band at the expected molecular mass. A representative example is depicted in Figure A.2, Appendix.

calponin or the Cy3-anti-α-SMA antibodies were omitted. After another three washing cycles in PBS, sections were mounted with glass coverslips using Fluoromount Aqueous Mounting Medium (Sigma-Aldrich).

Target	Host	Fluorophore	Dilution	Manufacturer
calponin-1	rabbit	none	1 : 200	Merck Millipore
α-SMA	rabbit	Cy3	1 : 200	Sigma-Aldrich
rabbit immunoglobulin	goat	Alexa Fluor 488	1 : 100	Invitrogen

Table 4.4.: Antibodies used for immunohistochemistry. A test run was conducted to ensure strong and specific vessel labeling, as depicted Figure A.3, Appendix.

4.4.2 Image Acquisition, Signal Quantification and Data Processing

Image acquisition was performed on an Axiovert 200M inverted microscope or an Axio Imager.M2 upright microscope via the AxioVs40 user interface (v4.8.2.0; all Zeiss, Oberkochen, GER). Both microscopes were using a mercury arc lamp as illumination source. Images from both calponin- and α-SMA-positive vessels with a diameter of either below 20 µm or above 40 µm were taken at 100× magnification in the channels corresponding to the three fluorophores used. The exposure time was kept constant within each group of samples to be compared.

Signals were quantified using the ImageJ (Fiji) software. Selections excluding lumen were drawn around the vessels to create a region of interest. The mean pixel intensity in each channel was measured. For calponin and α-SMA signals, background staining measured in an adjacent vessel-free region was subtracted. To correct for variance in cell density, values were normalized to the DAPI signal obtained from the same area.

4.5 Reverse-Transcriptase Quantitative PCR (RT-qPCR)

4.5.1 Sample Preparation

RNA extraction was performed using the RNeasy Mini Kit (Qiagen), which utilizes RNA binding to a silica membrane, according to the manufacturer's instructions, including a 15-minute incubation step with 80 µL DNase I (0.39 U/µL) at RT (RNase-free DNase Set, Qiagen). RNA was quantified using a NanoDrop ND-1000 spectrophotometer (Thermo Fisher Scientific). Reverse transcription to cDNA was conducted on 250 ng RNA using 2.86 µM oligo(dT)15 primers and the Omniscript RT Kit (Qiagen) according to the instructions provided by the supplier.

4.5.2 Primer Design and Quality Control

Primers were designed using either the *Universal Probe Library Probe Finder* web application (v2.50; Roche Diagnostics), the *RTPrimerDB*[1] or selected from literature sources. Non-intron-spanning primer pairs were excluded to avoid amplification of contaminant genomic DNA and the specificity of each primer pair was evaluated *in silico* using the *Primer-BLAST*[2] online application. An overview of primer sequences used in this project is given in Table 4.5.

4.5.3 qPCR Cycling Conditions

RT-qPCR was conducted in non-transparent white 384-well plates sealed with adhesive foil. Each well contained forward and reverse primers at a final concentration of 200 nM each, 6 µL of Brilliant II SYBR Green MasterMix (Agilent Technologies, Santa Clara, USA), 3.52 µL of DNAse-free water and 2 µL of cDNA, diluted 1 : 20 (v/v) in DNAse-free water.

[1] `http://medgen.ugent.be/rtprimerdb/index.php`; University of Ghent, Gent, BEL

[2] `https://www.ncbi.nlm.nih.gov/tools/primer-blast/`; National Center for Biotechnology Information, Bethesda, USA

Gene	Corresponding protein	Primer sequence
ACTA2	α-SMA	**F:** 5'-TCAATGTCCCAGCCATGTAT-3' **R:** 5'-CAGCACGATGCCAGTTGT-3'
ACTB	β-actin	**F:** 5'-AGAGCTACGAGCTGCCTGAC-3' **R:** 5'-CGTGGATGCCACAGGACT-3'
CD36	CD36 (thrombospondin receptor)	**F:** 5'-CCTCCTTGGCCTGATAGAAA-3' **R:** 5'-GTTTGTGCTTGAGCCAGGTT-3'
CD68	CD68	**F:** 5'-GTCCACCTCGACCTGCTCT-3' **R:** 5'-CACTGGGGCAGGAGAAACT-3'
CNN1	calponin 1	**F:** 5'-GCTGTCAGCCGAGGTTAAGA-3' **R:** 5'-CCCTCGATCCACTCTCTCAG-3'
COL1A1	collagen type I, α 1 subunit	**F:** 5'-GGGATTCCCTGGACCTAAAG-3' **R:** 5'-GGAACACCTCGCTCTCCA-3'
ELK1	ELK-1	**F:** 5'-GAAGAATCACACCCTTGGAA-3' **R:** 5'-GACAAAGGAATGGCTTCTCA-3'
ELK3	ELK-3 (SRF accessory protein 2)	**F:** 5'-AGCAGAGCCCTGCGATACTA-3' **R:** 5'-TCTCCGGGAAAGAGACAAACT-3'
ELK4	ELK-4 (SRF accessory protein 1)	**F:** 5'-CTCGAGTTTCCAGCGTGAG-3' **R:** 5'-CAGGGTGATAGCACTGTCCAT-3'
KLF4	Klf4	**F:** 5'-CCCAATTACCCATCCTTCCT-3' **R:** 5'-ACGATCGTCTTCCCCTCTTT-3'
KLF5	Klf5	**F:** 5'-AAACGACGCATCCACTACTGC-3' **R:** 5'-TTGTATGGCTTTTCACCAGTGTG-3'
LGALS3	galectin-3	**F:** 5'-CTTCTGGACAGCCAAGTGC-3' **R:** 5'-AAAGGCAGGTTATAAGGCACAA-3'
MKL1 (total)	MKL 1 total (both long and short mRNA isoforms)	**F:** 5'-CTCCAGGCCAAGCAGCTG-3' **R:** 5'-CCTTCAGGCTGGACTCAAC-3'
MKL2	MKL 2	**F:** 5'-AAAACTTACCCCCTCTGAACG-3' **R:** 5'-CTCTCGTCCTCCTTTGTTGC-3'
SRF	serum response factor (SRF)	**F:** 5'-AGCACAGACCTCACGCAGA-3' **R:** 5'-GTTGTGGGCACGGATGAC-3'

Table 4.5.: Primers used for RT-qPCR analysis. None of these primers bear any 5'- or 3'-terminal modifications. A test run was conducted with each set of primers to ensure sufficient abundance of the target mRNA and selective amplification based on the amplification curves and melting profiles, respectively. A representative example is depicted in Figure A.4, Appendix.

Samples were prepared either in duplicate or triplicate. As negative controls, a cDNA-free well (no template control; NTC) and a well loaded with non-reverse transcribed mRNA (no reverse transcriptase; NRT) were included.

Following a 10-minute activation plateau at 95° C each qPCR consisted of 40 cycles of denaturation for 30 s at 95° C, and primer hybridization and DNA synthesis for 1 minute at 60° C with a cooling rate of 2.5° C/s and a heating rate of 4.8° C/s. Runs were performed on a Roche LightCycler 480 II operated using the corresponding LightCycler 480 user software (v1.5.1; both Roche Diagnostics).

4.5.4 Data Analysis

Data were analyzed with the $2^{-\Delta\Delta C_{\mathrm{T}}}$ method as described by Schmittgen and Livak (2008) using *ACTB*[3] mRNA for normalization.

4.6 Statistics

Statistical analysis was performed using the Mann-Whitney U test. A probability value ≤ 0.05 was considered significant.

[3] *ACTB* encodes the β-actin protein.

5 Results

5.1 Pathogenic *HTRA1* Mutations Reduce TGF-β Signaling in Human Skin Fibroblasts

Beaufort et al. (2014) reported a strong decrease of phosphorylated Smad2/3 in the brain of *HTRA1*$^{-/-}$ mice (for the role of phosphorylated Smads in TGF-β signaling, see Section 3.2.1.3), as well as in primary skin fibroblasts of a CARASIL patient. These observations link *HTRA1* deficiency to a reduced TGF-β signaling activity.

To further investigate the link between HTRA1 and TGF-β signaling activity, I used skin fibroblasts of healthy controls as well as of homo- and heterozygous *HTRA1* mutation carriers (Section 4.1.1).

In a pilot experiment, I analyzed fibroblast lysates of one control individual and one homozygous mutation carrier by immunoblot using β-actin and tubulin as loading controls (Figure 5.1a). In line with the findings of Beaufort et al. (2014), phospho-Smad2/3 levels are strongly reduced in patient cells (Figure 5.1b, upper panel). To distinguish between reduced expression and reduced phosphorylation of the Smads, I also analyzed total Smad2 (Figure 5.1b, middle panel). No loss of Smad2 is detected in CARASIL patient cells, indicating hypophosphorylation. I subsequently investigated the expression of CTGF, another well-established surrogate marker of TGF-β signaling activity (Figure 5.1b, lower panel). In good congruence with Smad2 phosphorylation pattern, a strongly reduced CTGF expression is found in CARASIL patient cells, confirming reduced TGF-β signaling activity.

To extend these observations to a larger sample of patient-derived skin fibroblasts in-

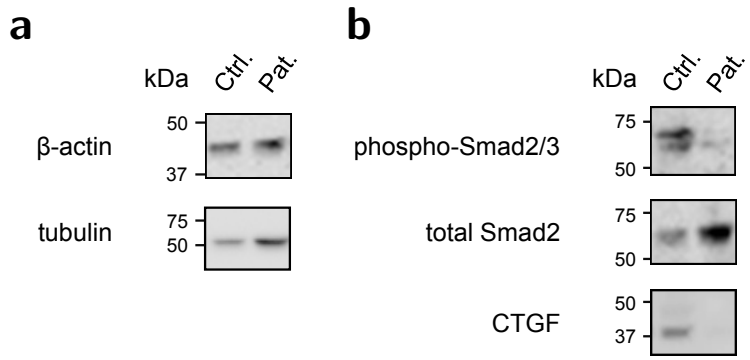

Figure 5.1.: TGF-β signaling activity in skin fibroblasts of a CARASIL patient

Skin fibroblast lysates of one healthy control individual (Ctrl.) and one homozygous *HTRA1* mutation carrier (Pat.) were analyzed by immunoblot using antibodies directed against (**a**) β-actin (upper panel) and tubulin (lower panel) used as loading controls as well as (**b**) phospho-Smad2/3 (upper panel), total Smad2 (middle panel) and CTGF (lower panel). Based on their molecular mass, the upper and lower bands detected by the phospho-Smad2/3 antibody correspond to phospho-Smad 2 and -3, respectively.

cluding cells from heterozygous mutation carriers, I performed immunoblot analysis of the aforementioned proteins on 13 different lysates derived from 5 control, 5 heterozygous and 3 homozygous skin fibroblast cultures. The characteristics of the corresponding patients are provided in Section 4.1.1. For statistical analysis, a fourth group was taken into account, comprising the data of all mutation carriers (pooled homo- and heterozygous patients).

In both homo- and heterozygous mutation carrier cells, the abundance of phospho-Smad2 is reduced, albeit not significantly (Figure 5.2a), while total Smad2 levels are unchanged (Figure 5.2b). This indicates Smad2 hypophosphorylation, as reflected by the phospho-/total Smad2 ratios (Figure 5.2c). Of note, Smad hypophosphorylation is as pronounced in hetero- as in homozygous patient cells. Similar to Smad2 phosphorylation, CTGF is drastically reduced in *HTRA1* mutation carrier cells, however, significance is only reached in heterozygous carriers.

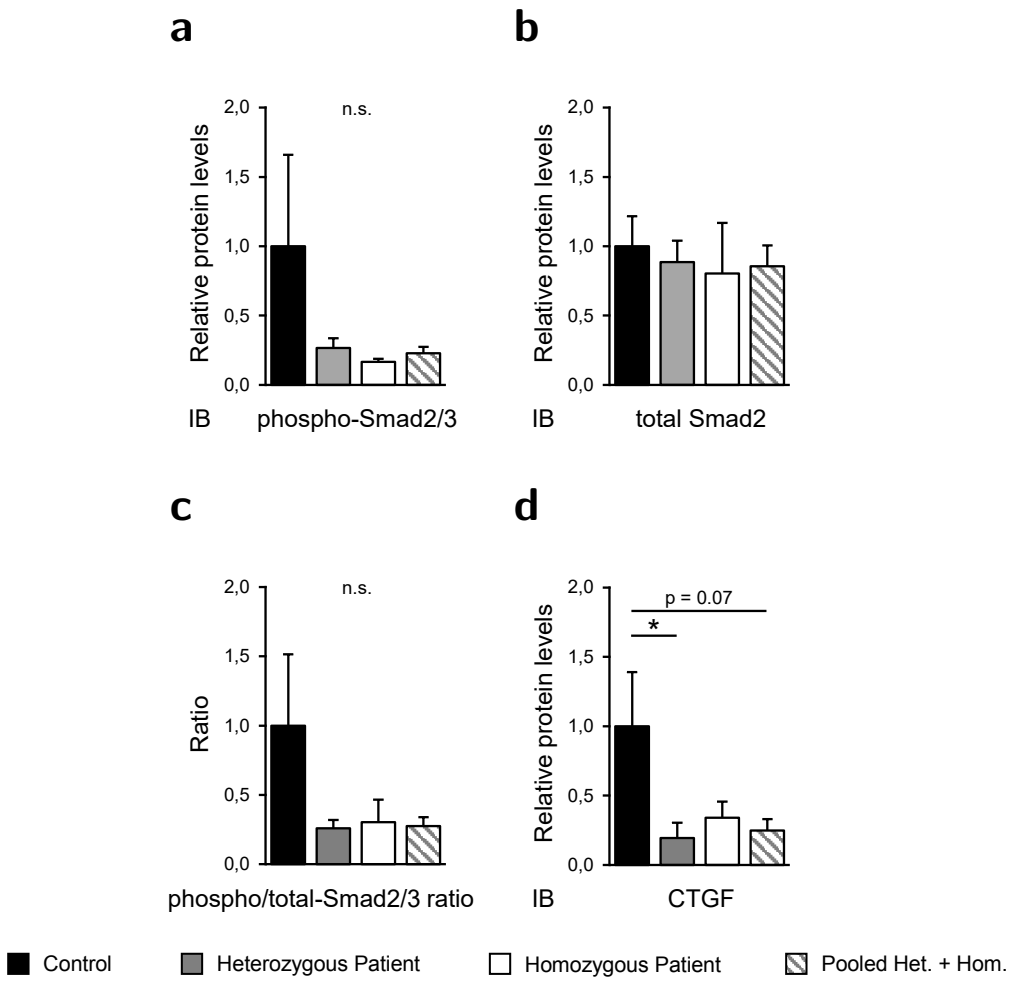

Figure 5.2.: TGF-β signaling in a larger sample of human skin fibroblasts

Human skin fibroblast lysates were analyzed by immunoblot using antibodies against (**a**) phospho-Smad2/3, (**b**) total Smad2, and (**d**) CTGF. Tubulin was used for normalization. (**c**) A phospho-/total Smad2/3 ratio was calculated. $n = 5$ healthy control individuals, $n = 5$ heterozygous patients, $n = 3$ homozygous patients and $n = 8$ pooled samples of heterozygous and homozygous patients. Mean values obtained from control cells were set to 1. Results are displayed as mean + standard error of the mean (SEM). $*p \leq 0.05$ (Mann-Whitney U test).

Altogether these findings point to a considerable impairment of TGF-β signaling in cells carrying pathogenic *HTRA1* mutations.

5.2 Pathogenic *HTRA1* Mutations Impair the Contractile Phenotype of Human Skin Fibroblasts

TGF-β plays a fundamental role in cell differentiation including the acquisition of a contractile phenotype (Section 3.2.1.3). Hence, I set out to investigate the contractile phenotype of the fibroblast cultures described in the previous section.

I first analyzed the expression of key contractile phenotype markers by immunoblot and/or RT-qPCR. These include α-SMA, an early marker of contractile differentiation, as well as calponin-1 and SM22, both intermediate differentiation markers. I also investigated the expression of integrin β1, an adhesion receptor involved in various processes, including contraction. Protein levels of α-SMA, SM22 and integrin β1 were significantly lower in heterozygous patients, while their reduction in homozygous patients did not reach significance (Figure 5.3a-d). Protein and mRNA levels of calponin-1 were decreased in all groups, albeit not significantly. These data are in agreement with TGF-β signaling activity results.

To confirm a functional deficit, I next assessed cell contractility. For this, fibroblasts were cast in a gel made of type I collagen, followed by gel contraction measurements (a typical example is depicted in Figure 5.4a) at different time points. As depicted in Figure 5.4b, control cells efficiently contract the gel over time, while this ability is lost in patient cells. In parallel, the metabolic activity of cells seeded in independent wells was measured via MTT assay to account for differences in viable cell number (Figure 5.4c). Systematic analysis of control, hetero- and homozygous mutation carrier fibroblasts revealed that cells from heterozygous patients display a reduced contractility / metabolic activity ratio (Figure 5.4d).

Together, contractile protein expression profiles and functional contraction assays both link heterozygous pathogenic *HTRA1* mutations to a loss of contractile phenotype in pri-

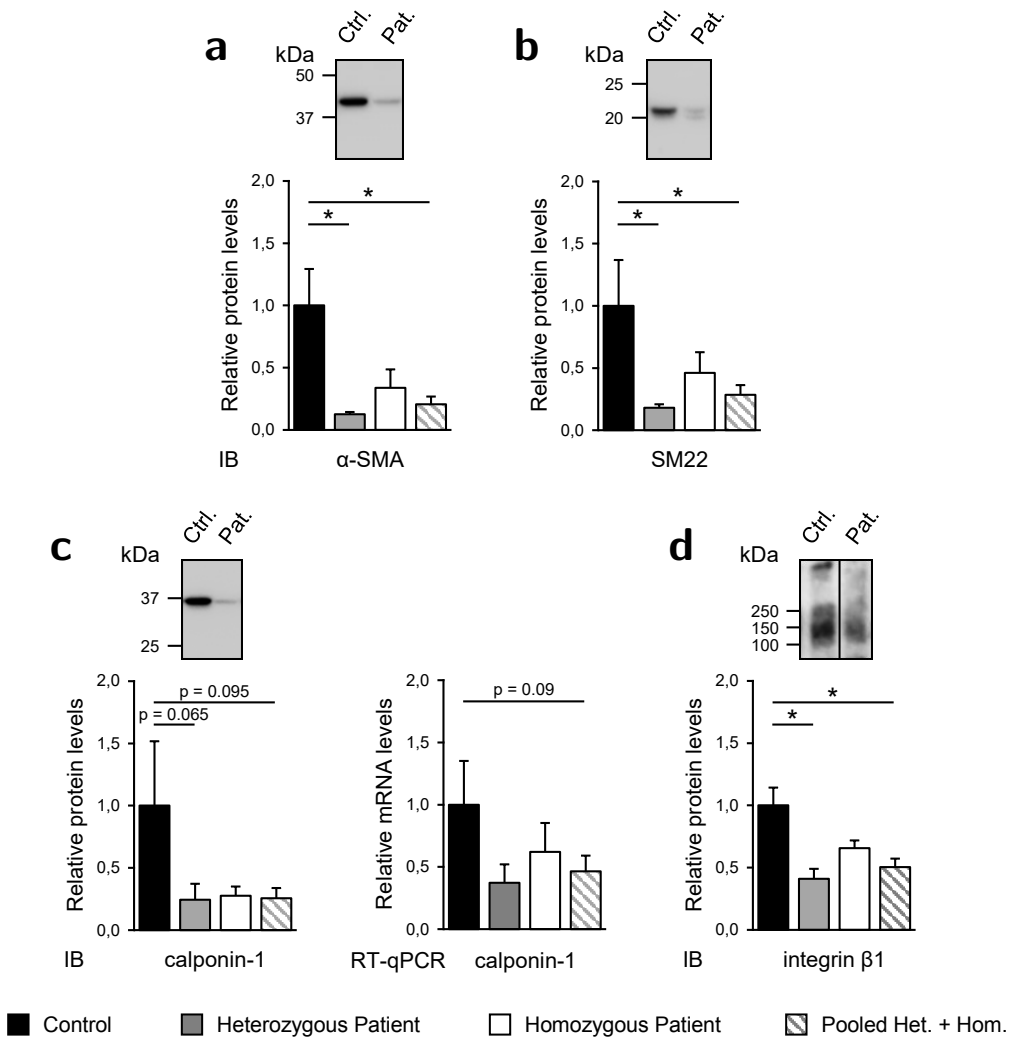

Figure 5.3.: Contractile marker expression in human skin fibroblasts

Human skin fibroblast lysates were analyzed by immunoblot using antibodies against (**a**) α-SMA, (**b**) SM22, (**c**, left panel) calponin-1 or (**d**) integrin β1. Signal intensity was quantified using tubulin for normalization. (**c**, right panel) Calponin-1 mRNA in fibroblast extracts was quantified by RT-qPCR, using β-actin for normalization ($n = 5$ healthy control individuals, $n = 5$ heterozygous patients, $n = 3$ homozygous patients, $n = 8$ pooled samples of heterozygous and homozygous patients). Mean values of control cells were set to 1. Results are displayed as mean + SEM. $*p \leq 0.05$ (Mann-Whitney U test).

mary skin fibroblasts.

5.3 Pathogenic *HTRA1* Mutations Promote Cell Phagocytic Phenotype in Human Skin Fibroblasts

As described in Section 3.3.3.1, loss of contractile phenotype is classically associated with a gain of synthetic phenotype. To evaluate this possibility, I quantified the expression of synthetic phenotype markers including the ECM proteins type I collagen (Figure 5.5a) and fibronectin (Figure 5.5b), as well as that of the cell-cell adhesion receptor connexin 43 (Figure 5.5c) by immunoblot or RT-qPCR. None of these markers appear to be affected by *HTRA1* mutations, thereby excluding cell switching towards a synthetic phenotype.

Recently, the loss of VSMC contractile phenotype in atherosclerotic lesions was reported to be paired with a gain of a phagocytic phenotype, observed in the form of galectin-3 and CD68 upregulation. Similarly, I found significantly elevated mRNA levels of both markers in cells from heterozygous patients (Figure 5.6a and b). Additionally, CD36, a hallmark macrophage phagocytosis-related receptor is moderately, but not significantly, upregulated (Figure 5.6c).

Together, these observations indicate that loss of the contractile phenotype in heterozygous *HTRA1* mutation carrier cells comes along with an upregulation of markers associated with phagocytosis. Whether this expression profile correlates with an increased phagocytic capacity, remains to be determined.

5.4 Pathogenic *HTRA1* Mutations Affect the Transcriptional Differentiation Program in Human Skin Fibroblasts

To further understand the mechanisms that mediate cell reprogramming in *HTRA1* mutation carrier cells, I analyzed transcriptional pathways involved in cell differentiation (see Section 3.3.4.2), focusing on those affected by TGF-β.

SRF levels, measured by RT-qPCR, are elevated in heterozygous, but not in homozygous

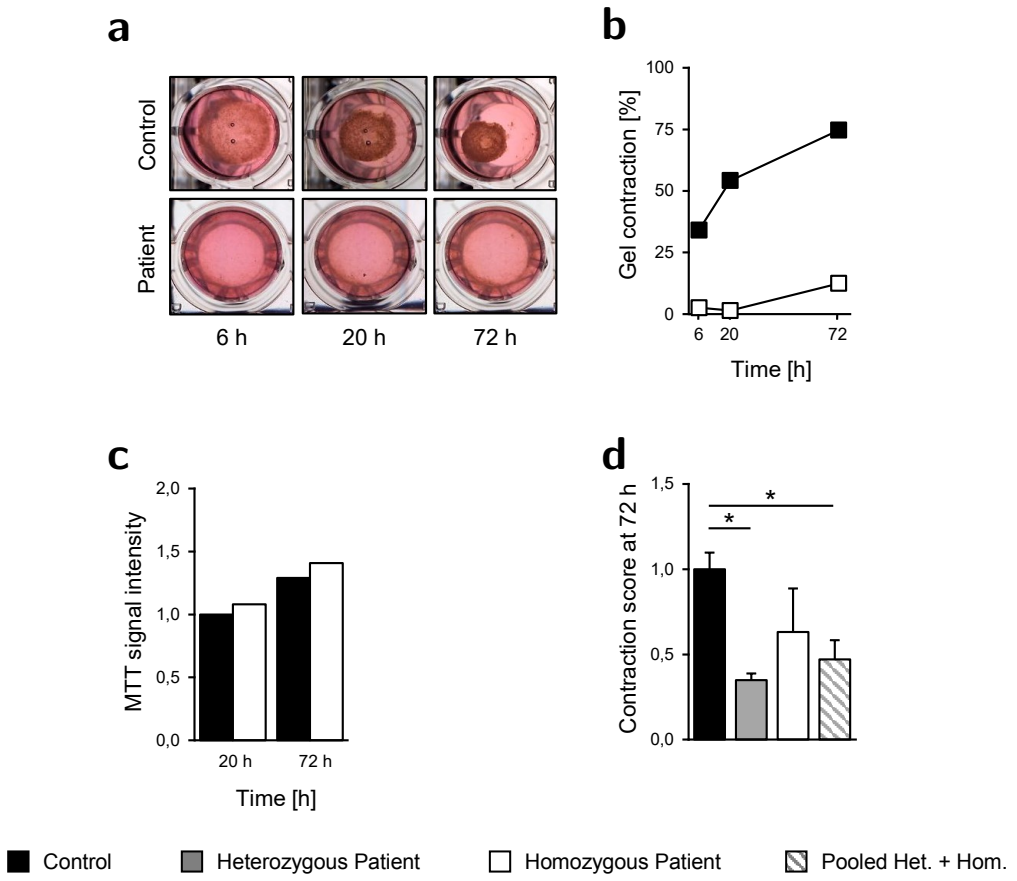

Figure 5.4.: Assessment of contractility in human skin fibroblasts

a-c Contractility assay of one healthy control and one patient cell culture. (**a**) Picture and (**b**) quantification of fibroblast-induced contraction of type I collagen gel, which manifests as a progressive reduction of gel surface. (**c**) MTT metabolic activity assay (arbitrary units). (**d**) Contraction scores – taking into account contraction and viability – determined at 72 h ($n = 5$ healthy control individuals, $n = 5$ heterozygous patients, $n = 3$ homozygous patients, $n = 8$ pooled samples of heterozygous and homozygous patients). Mean values of controls were set to 1. Results are displayed as mean + SEM. $*p \leq 0.05$ (Mann-Whitney U test).

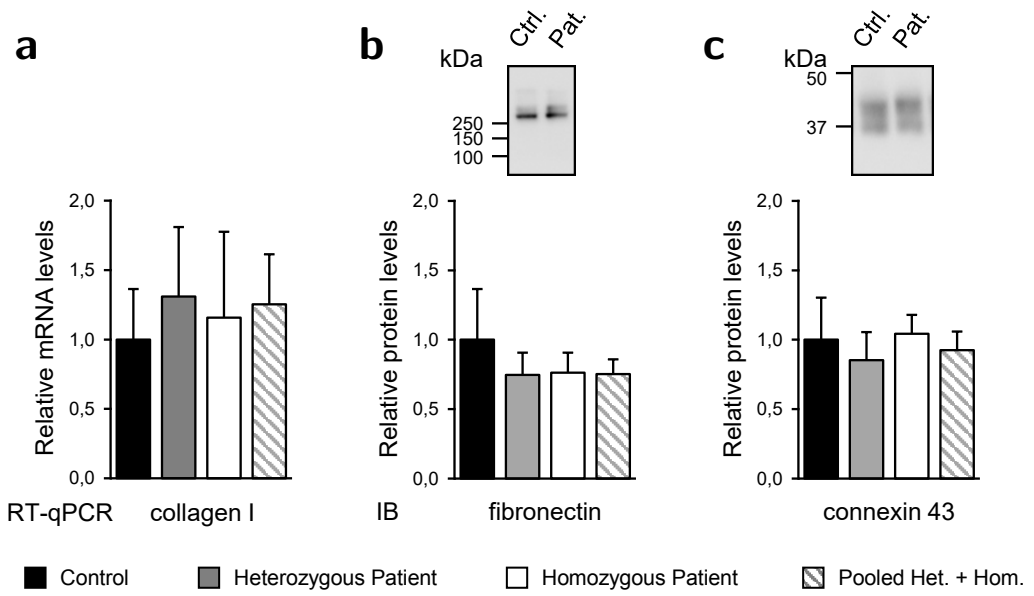

Figure 5.5.: Expression of synthetic phenotype markers in *HTRA1* mutation carrier fibroblasts

(**a**) Collagen I mRNA was quantified by RT-qPCR and β-actin was used for normalization. Human skin fibroblast lysates were analyzed by immunoblot using antibodies against fibronectin (**b**) and connexin 43 (**c**). Here, tubulin was used for normalization following signal quantification ($n = 5$ healthy control individuals, $n = 5$ heterozygous patients, $n = 3$ homozygous patients, $n = 8$ pooled samples of heterozygous and homozygous patients). Mean values of controls were set to 1. Results are displayed as mean + SEM. $*p \leq 0.05$ (Mann-Whitney U test).

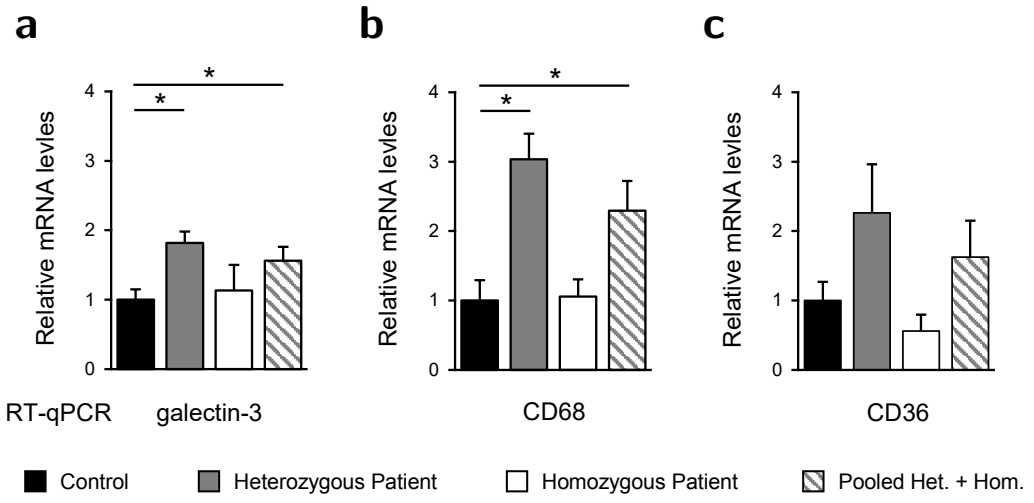

Figure 5.6.: Expression of phagocytic phenotype markers in human skin fibroblasts

RT-qPCR was used to quantify mRNA levels of (**a**) galectin-3, (**b**) CD68, and (**c**) CD36 in human skin fibroblast extracts. β-actin was used for normalization ($n = 5$ healthy control individuals, $n = 5$ heterozygous patients, $n = 3$ homozygous patients, $n = 8$ pooled samples of heterozygous and homozygous patients). Mean values of controls were set to 1. Results are displayed as mean + SEM. $*p \leq 0.05$ (Mann-Whitney U test).

patient cells (Figure 5.7a).

The expression of the SRF partner myocardin, a known activator of the contractile phenotype, displays minimal, if any reduction (Figure 5.7b). mRNA levels of the myocardin cofactor MKL 1 are largely unchanged (Figure 5.7c). Similar to SRF, MKL 2 mRNA is increased in heterozygous mutation carriers exclusively, although just short of significance (Figure 5.7d).

Members of the ternary complex factor (TCF) family, which are potent antagonists of the SRF-myocardin axis, were also analyzed. Among these, Elk-1 and -3 expression is upregulated by a factor of 2-3 exclusively in heterozygous mutation carrier cells (Figure 5.8a and b). In contrast, Elk-4 levels remain unaffected across groups (Figure 5.8c).

These data are compatible with an impairment of the SRF-myocardin axis in heterozygous cells. The homozygous group, however, and in contrast to most other markers examined, did not display any distinguishable trend regarding TCF expression. Here, the recent observation that Krueppel-like factors (Klfs) not only repress the contractile phenotype, but also induce phagocytic marker expression motivated us to consider these factors as promising candidates.

RT-qPCR analysis shows a 2.6- to 3.3-fold elevation of Klf4 expression spread across both hetero- and homozygous patient cells, although significance is only observed in heterozygous cells (Figure 5.9a). In contrast, Klf5 expression is reduced in both cell types.

Notably and in addition to being significant, Klf4 upregulation appears well-correlated to the reduction of TGF-β signaling and to the loss of contractile markers.

Together, these data suggest that Klf4 upregulation might mediate reprogramming of heterozygous patient cells from a contractile towards a phagocytic phenotype as a consequence of impaired TGF-β signaling.

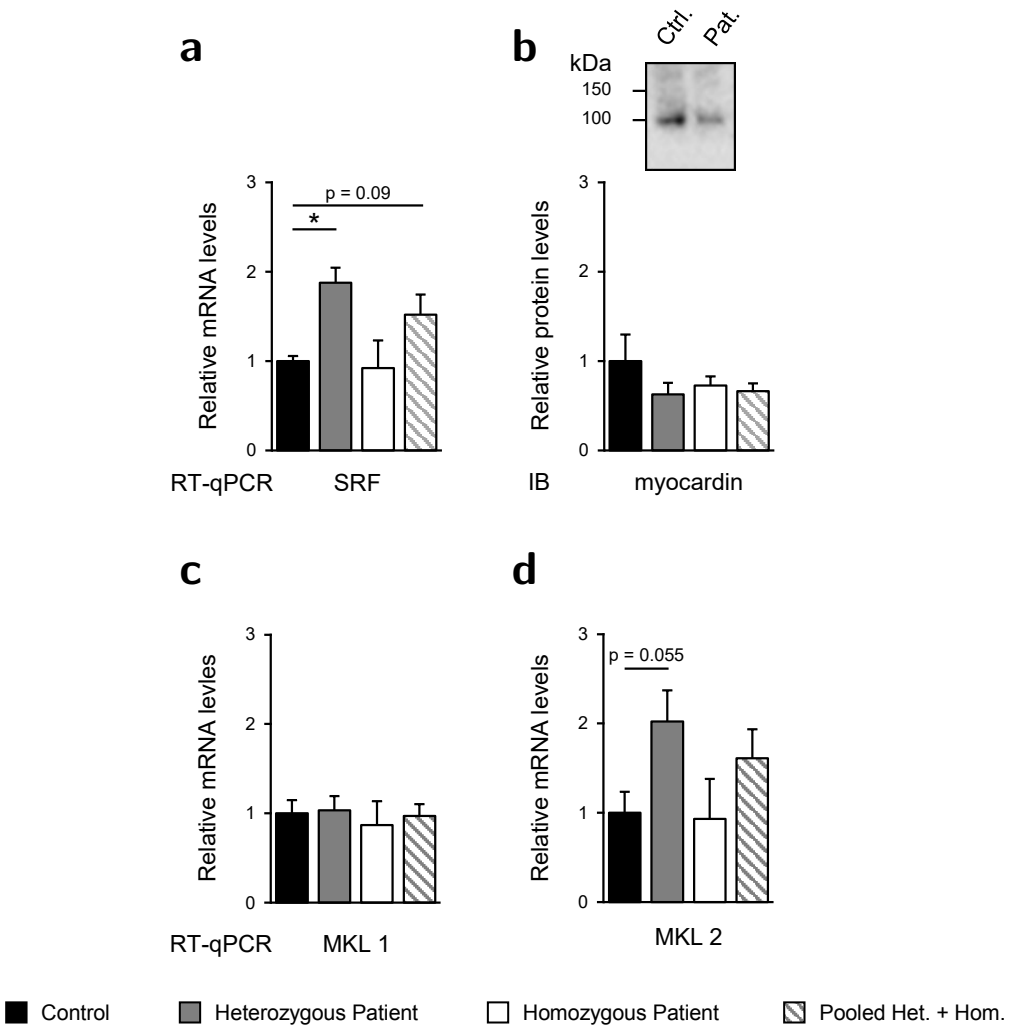

Figure 5.7.: Expression of members of the SRF-myocardin axis in *HTRA1* mutation carrier fibroblasts

(**a**) SRF, (**c**) MKL 1, and (**d**) MKL 2 mRNA was quantified by RT-qPCR using β-actin for normalization. Human skin fibroblast lysates were analyzed by immunoblot using antibodies against myocardin (**b**). Here, tubulin was used for normalization ($n = 5$ healthy control individuals, $n = 5$ heterozygous patients, $n = 3$ homozygous patients, $n = 8$ pooled samples of heterozygous and homozygous patients). Mean values of controls were set to 1. Results are displayed as mean + SEM. $*p \leq 0.05$ (Mann-Whitney U test).

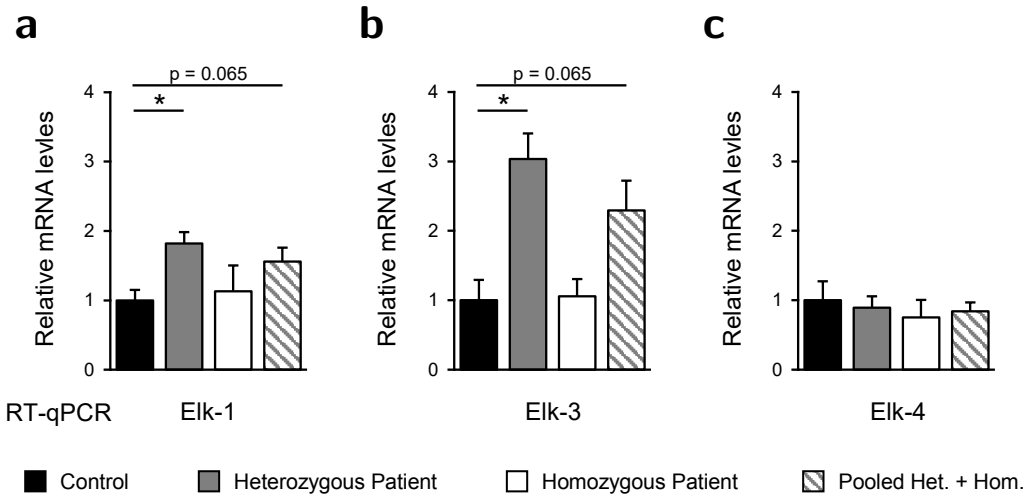

Figure 5.8.: Expression of TCFs in *HTRA1* mutation carrier fibroblasts

RT-qPCR was used to quantify mRNA levels of (**a**) Elk-1, (**b**) Elk-3, and (**c**) Elk-4 in fibroblast extracts. β-actin was used for normalization ($n = 5$ healthy control individuals, $n = 5$ heterozygous patients, $n = 3$ homozygous patients, $n = 8$ pooled samples of heterozygous and homozygous patients). Mean values of controls were set to 1. Results are displayed as mean + SEM. $*p \leq 0.05$ (Mann-Whitney U test).

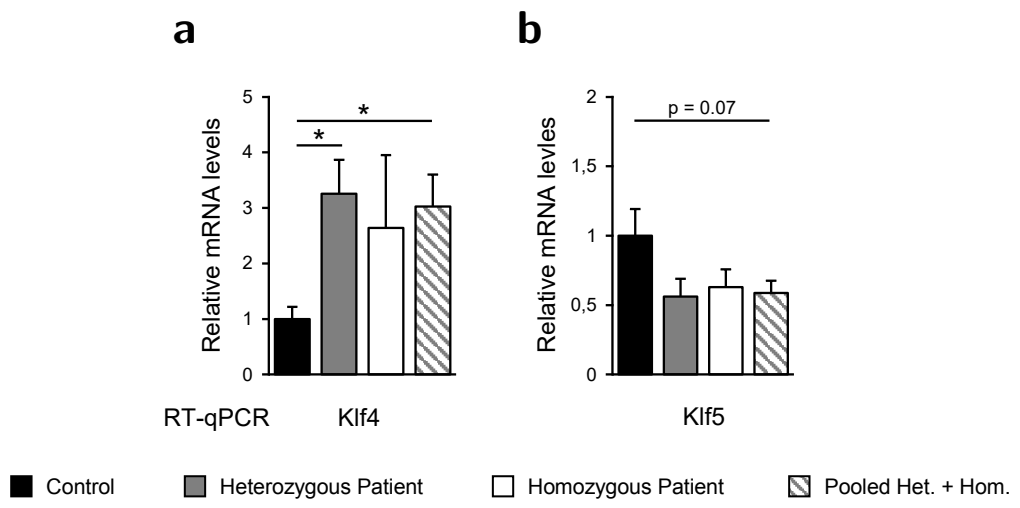

Figure 5.9.: Expression of Klfs in *HTRA1* mutation carrier fibroblasts

RT-qPCR was used to quantify mRNA levels of (**a**) Klf4, and (**b**) Klf5 in human skin fibroblasts. β-actin was used for normalization ($n = 5$ healthy control individuals, $n = 5$ heterozygous patients, $n = 3$ homozygous patients, $n = 8$ pooled samples of heterozygous and homozygous patients). Mean values of controls were set to 1. Results are displayed as mean + SEM. $*p \leq 0.05$ (Mann-Whitney U test).

5.5 *HTRA1*-Deficiency Reduces the Expression of Contractile Phenotype Markers in Mouse Cerebrovasculature

To confirm these findings *in vivo*, I made use of *HTRA1*$^{-/-}$ mice (Section 4.2.1). These animals display no striking phenotype beside a reduced TGF-β signaling activity, as reported in brains of 2-12-month old animals (Beaufort et al., 2014).

First, I performed immunoblot analysis of contractile phenotype marker expression in full brain lysates (for specifications see Section 4.2.4) of 2-24-month old *HTRA1*$^{+/+}$ and *HTRA1*$^{-/-}$ mice. *HTRA1*$^{-/-}$ animals display an average decrease of calponin-1 expression by 28 %, ranging from 20 % in young animals (2-3 months) to 32 % in older animals (12-24 months, Figure 5.10a). In contrast, α-SMA, SM22 and SM-MHC show no clear reduction in *HTRA1*$^{-/-}$ animals (Figure 5.10b-d).

Subsequently, mouse brain sections were subjected to immunohistochemical analysis using anti-calponin-1 and anti-α-SMA antibodies. Vessels positive for both markers were selected and sorted by size. Vessels with a diameter below 20 µm were classified as "small" vessels, while those with a diameter over 40 µm were grouped as "large" vessels. Analysis of 2- and 7.5-month old mice revealed no impact of *HTRA1* deficiency (not illustrated). In contrast, in 12-month old animals, a clear reduction of both calponin-1 and α-SMA levels is detected in small vessels of *HTRA1*$^{-/-}$ animals (Figure 5.11). In larger vessels (including meningeal ones), loss of contractile protein is not significant. Notably, this apparent correlation of vessel diameter to loss of contractile markers suggests that other methods such as immunoblot, where vessel size is not considered, likely underestimate the impact of of *HTRA1* deficiency on cell phenotype.

Together, these data indicate a loss of contractile proteins that appears to be restricted to small vessels in *HTRA1*-deficient animals of advanced age.

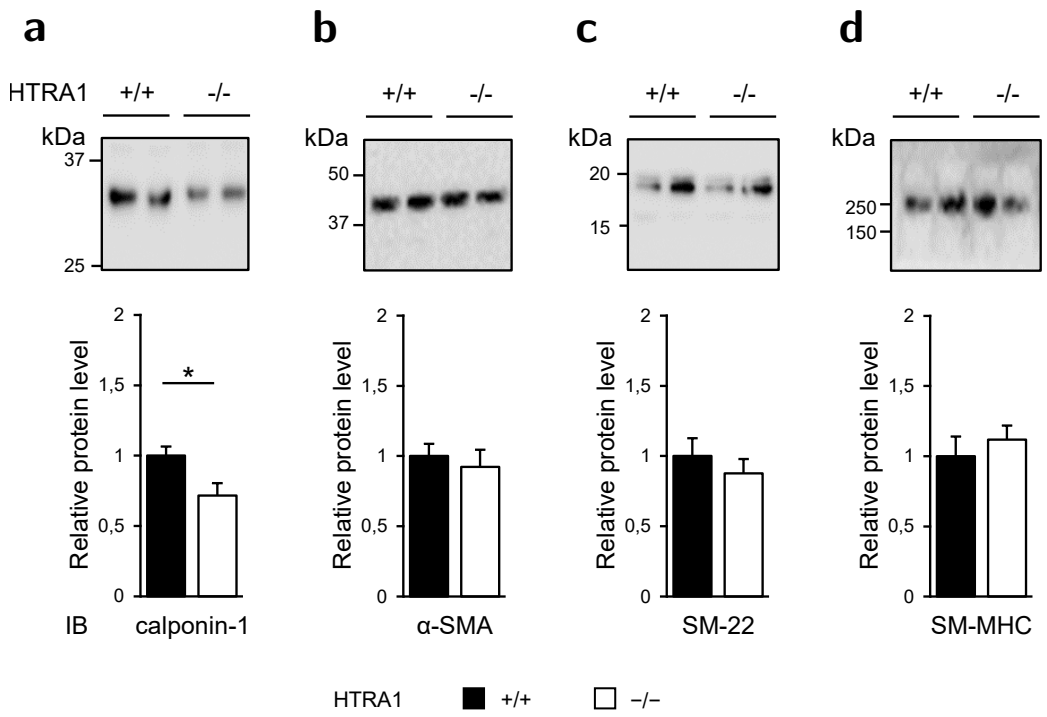

Figure 5.10.: Expression of contractile phenotype markers in full brain lysate of *HTRA1*$^{+/+}$ and $^{-/-}$ mice

Mouse full brain lysates were analyzed by immunoblot using antibodies against (**a**) calponin-1, (**b**) α-SMA, (**c**) SM22, and (**d**) SM-MHC. β-actin was used for normalization (n = 11 *HTRA1*$^{+/+}$ mice and n = 11 *HTRA1*$^{-/-}$ mice) Mean values of *HTRA1*$^{+/+}$ animals were set to 1. Results are displayed as mean + SEM. $*p \leq 0.05$ (Mann-Whitney U test).

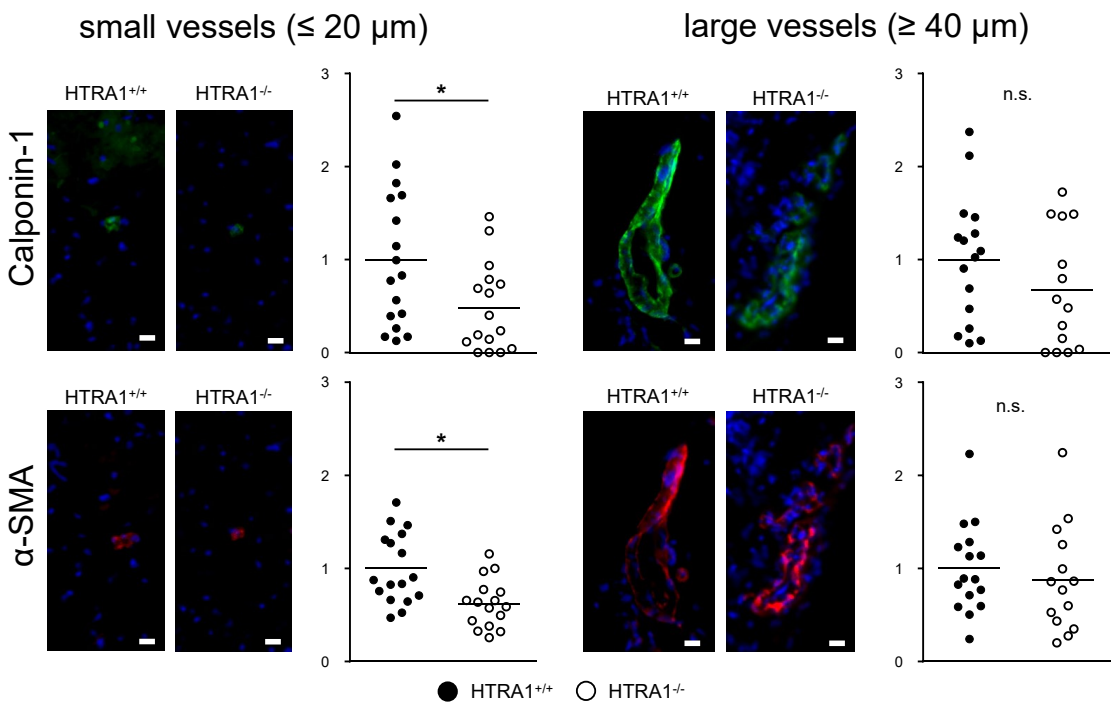

Figure 5.11.: Immunohistochemical analysis of contractile phenotype markers in mouse cerebrovasculature

Mouse brain sections underwent immunohistochemical analysis using primary antibodies against calponin-1 (top row) and α-SMA (bottom row). Following secondary antibody application and signal intensity quantification, DAPI was used for normalization. 14-17 vessels per group from $n = 4$ *HTRA1*$^{+/+}$ mice and $n = 4$ *HTRA1*$^{-/-}$ mice aged 12-14 months. Horizontal bars indicate mean values. Mean values of *HTRA1*$^{+/+}$ were set to 1. $*p \leq 0.05$; n.s. $p > 0.05$ (Mann-Whitney U test). Scale bar in the example images for each group, vessel size and antibody indicates 20 µm.

5.6 TGF-β-Mediated Rescue of Contractile Cell Function

In a proof-of-principle assay to rescue contractile cell function, I exposed skin fibroblasts to recombinant TGF-β.

As expected, treatment of control cells results in a dose-dependent increase of the contractile phenotype markers calponin-1, α-SMA and SM22 (Figure 5.12a). Furthermore, the ECM protein fibronectin, a known target of TGF-β signaling, is upregulated as well (Figure 5.12b), whereas PDGF receptor β (PDGFR-β), the expression of which is not known to be affected by TGF-β signaling, remains unchanged (Figure 5.12c).

Importantly, homo- and heterozygous patient cells are also responsive to TGF-β treatment, resulting in an upregulation of contractile and ECM markers (Figure 5.12a and b).

Moreover, in a pilot experiment including one healthy control and one homozygous patient cell culture, I could evidence that TGF-β stimulation increases the contractility of both control and patient cells (Figure 5.12d).

Together, these observations suggest that it is possible to restore the contractile properties of *HTRA1* mutation carrier fibroblasts by treatment with TGF-β.

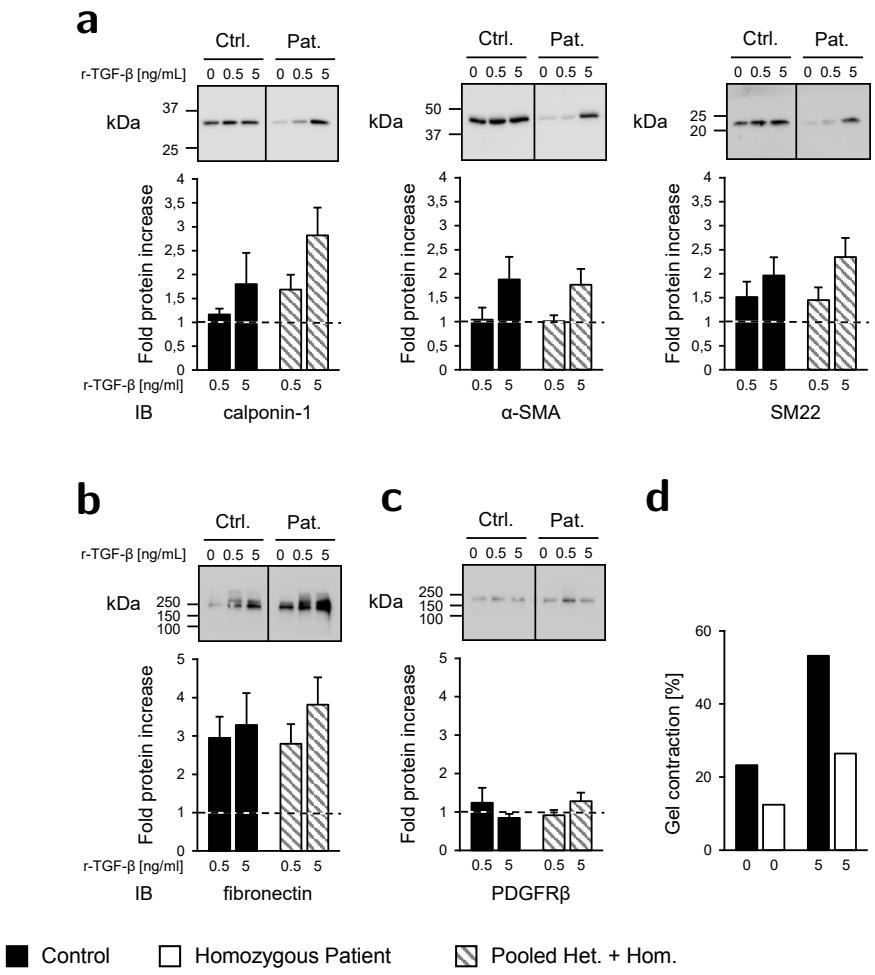

Figure 5.12.: TGF-β treatment restores phenotype and function of cultured human skin fibroblasts

(**a**-**c**) Immunoblot analysis of human skin fibroblasts after stimulation with recombinant TGF-β (r-TGF-β). Antibodies used were directed against calponin-1 (**a**, left panel), α-SMA (**a**, middle panel), SM22 (**a**, right panel), fibronectin (**b**), and PDGFR-β (**c**). Tubulin was used for normalization and unstimulated samples were set to 1 ($n = 5$ healthy control individuals, $n = 7$ pooled samples of heterozygous and homozygous patients). Results are displayed as mean + SEM. (**d**) Contraction of type I collagen gel by one healthy control and one patient skin fibroblast culture, with and without TGF-β treatment.

6 Discussion

Using a unique collection of primary fibroblasts from patients bearing *HTRA1* mutations, I have assembled data shedding new light on the pathomechanisms underlying *HTRA1*-related SVD (see Figure 6.1).

First, I established that loss of HTRA1 function correlates with a decrease in TGF-β signaling (see Section 5.1).

Second, I evidenced phenotypic switching in patient cells (see Sections 5.2 and 5.3). This includes a loss of contractile proteins, a reduction of the cell contractile function, and an upregulation of phagocytosis-associated markers. Importantly, a reduction of contraction markers was confirmed in the brains of HTRA1-deficient mice (see Section 5.5).

Third, I analyzed various transcriptional pathways highlighting Klf4 as a putative orchestrator of TGF-β signaling-related patient cell reprogramming (see Section 5.4).

Fourth, my analysis of hetero- as well as homozygous patient cell cultures indicated pathological alterations in both cell types. This observation is in good accordance with the recent identification of heterozygous *HTRA1* mutations in familial SVD sample groups (Verdura et al., 2015; Nozaki et al., 2016).

Fifth, I provide proof of principle for the rescue of TGF-β signaling and contractility in patient cells, e.g. via TGF-β treatment, an observation with therapeutic potential (see Section 5.6).

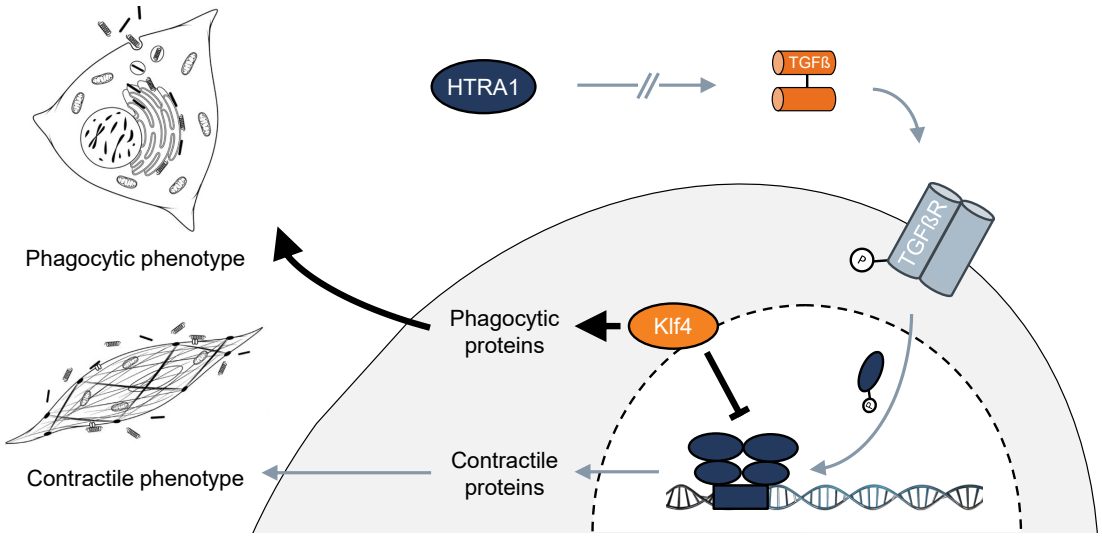

Figure 6.1.: Overview of the proposed pathomechanism in *HTRA1*-related SVD

Under normal circumstances, HTRA1 facilitates TGF-β signaling, ultimately resulting in the expression of proteins needed for contractile cell differentiation. Upon HTRA1 loss-of-function, a lack of TGF-β signaling fails to counterbalance repression of the contractile transcription program through Klf4. Hence, phagocytic protein expression stimulated by Klf4 produces a phagocytic cell phenotype. For a detailed description of HTRA1-mediated release of TGF-β and subsequent signal transduction as well as transcription, see Figures 3.5 and 3.8.

6.1 TGF-β Signaling

Over the course of my experimental work, I demonstrated a downregulation of TGF-β signaling in patient skin fibroblasts (see Section 5.1), thereby extending the observations of Beaufort et al. (2014). While these findings stand in good congruence with the loss of contractile markers and function I also observed in patient cells, they conflict with earlier descriptions made by Hara et al. (2009). Based on immunohistochemical analysis of patient brain, these authors proposed a role for *HTRA1* as a repressor of TGF-β and suspected elevated levels of TGF-β as well as its downstream targets to contribute to the disease. However, these conclusions were drawn from a very limited number of samples. Furthermore, the tissue used for analysis was obtained by autopsy, where ischemia-associated fibrosis and therefore excess TGF-β signaling would be expected as a consequence of the advanced stage of the disease rather than a cause.

Dysregulation of the TGF-β signaling pathway is an emerging common denominator for a broad variety of vascular disorders (see also Section 3.2.1.3) including several SVDs other than *HTRA1*-related SVD. For instance, *incontinentia pigmenti* (OMIM: 308300), a genodermatosis causing – among other pathologies – cerebral arteriopathy with vascular occlusions in newborns, is caused by mutations in the gene encoding IκB kinase γ (IKKγ/NEMO), a close interaction partner of TGF-β (de Groof, 2008; Smahi et al., 2000; Kim et al., 2014). Further examples include CADASIL, where an accumulation of LTBP-1 and TGF-β was observed within the vessel walls of patients (Kast et al., 2014). However, in these and many other diseases with potential involvement of TGF-β, it often remains to be examined whether and to which degree TGF-β signaling is up- or downregulated and which impact on its downstream targets ensues.

Upon close examination, it appears that diseases with a pathological upregulation of TGF-β seem to outweigh those with a loss of TGF-β signaling activity. This imbalance is further amplified when considering that disruption of the TGFBR may lead to net increase in signaling activity, due to the complex regulatory mechanisms involved. However, those regulatory mechanisms may at the same time account for some seemingly paradoxical path-

omechanisms. Consequently, antagonistic defects could result in comparable pathogenic remodeling as observed for cardiac and other developmental defects (Ishtiaq Ahmed et al., 2014).

6.2 Phenotypic Switching

My data link the lack of functional *HTRA1* to an aberrant cell phenotype and function, including a loss of contractility and a gain of phagocytosis-related markers. This observation led us to propose that – likewise to a number of other vascular disorders – phenotypic alterations of contractile cells might not only be a hallmark of *HTRA1*-related SVD, but a crucial pathomechanism as well, as has also been proposed by Ikawati et al. (2018), albeit in a different tissue (i.e., aorta) and with a different phenotypic outcome (i.e., synthetic shift).

TGF-β signaling is known to maintain cells in a highly differentiated, contractile state. It is thus tempting to speculate that the disruption of TGF-β signaling in *HTRA1*-deficient cells might be causative for the aforementioned aberrant cell phenotype. However, among others, PDGF and Wnt signaling are involved in contractile cell differentiation as well (Owens et al., 2004; Wang et al., 2015). Future work should thus aim at analyzing these and other signaling pathways to evaluate the diversity and specificity of the mechanisms involved in phenotypic switching in *HTRA1*-related SVDs.

Since loss of contractile markers and aberrant TGF-β expression have both been reported in cerebral arteries from CADASIL cases as well, indicators of phenotypic switching in this condition could be a worthwhile target for future research. Notably, in addition to skin biopsies from CADASIL patients (which are routinely acquired for diagnostic purposes), patient brain tissue from autopsy cases, as well as several mouse models are available, facilitating further investigation.

6.2.1 Contraction Markers and Contractile Function

I have identified a loss of various contractile markers (e.g. α-SMA, SM22 and calponin-1) in *HTRA1* mutation carrier cells and in the cerebrovasculature of *HTRA1*$^{-/-}$ mice. Hence, I demonstrated a reduced cell contractility *ex vivo*. Similar observances have been made in various other vascular disorders and pathogenic environments such as dyslipidemia, subarachnoid hemorrhage, and the hereditary SVD CADASIL (Sunaga et al., 2016; Ohkuma et al., 2003; Zhang et al., 2012) as well as, more recently, in aortic VSMCs of *HTRA1*$^{-/-}$ mice (Ikawati et al., 2018).

The precise functional shortcomings of cerebral VSMC and their contribution to cognitive decline in cerebrovascular disease are still not fully understood. One key mechanism is arguably defective neurovascular coupling, i.e. the regulation of blood flow and therefore neuronal metabolism through modulation of vascular tone in response to stimuli such as CO_2 and NO. Observations of impaired neurovascular coupling have, for example, been made in the vicinity of prior subarachnoid hemorrhage (Balbi et al., 2017).

Last, the de-differentiated state of VSMC due to impaired TGF-β signaling may be further augmented through ensuing disruption of feedback mechanisms. α-SMA, for instance, has been shown to contribute to the maintenance of the contractile VSMC phenotype through suppression of the GTPase Rac (Chen et al., 2016).

6.2.2 Phagocytosis-Associated Markers

I evidenced an upregulation of phagocytosis-related markers in patient cells. Phenotypic switching from a contractile to a synthetic phenotype has been well described in an array of vascular disorders and was recently suggested to occur in CARASIL (see Section 3.3.3.1 and Ikawati et al. (2018)). Conversely, modulation towards a phagocytic phenotype is a rather novel concept. Consequently, whether switching towards a phagocytic phenotype also takes place *in vivo*, will need to evaluated using e.g., *HTRA1*$^{-/-}$ and *HTRA1*$^{+/-}$ mouse tissue.

One of the questions arising from my observations is whether phagocytosis-associated

marker expression in *HTRA1* mutation carrier cells results in an actual gain of phagocytic function. Furthermore, if phagocytic activity is truly increased, it would be of interest to identify the substrates involved. Here, phagocytosis assays using latex beads with Fluorescein-based labelling might help shed some light on these mechanisms. Finally, it is also of interest to identify which, if any at all, antigens are presented on the contractile cell surface as a result of pathological phagocytic activity, should it take place.

6.2.3 Klf4

Based on my analysis of transcriptional pathways known to regulate contractile cells differentiation, I propose that Klf4 is a critical orchestrator of patient cell reprogramming. Despite the fact that the precise interaction and regulation of Klf4 and TGF-β is not yet entirely understood, a number of connections have been made. For instance, in an oncological context, studies have shown excessive TGF-β signaling upon loss of Klf4, thus suggesting a feedback mechanism between the two (Yao et al., 2016; Sun et al., 2017).

Moreover, as mentioned in Section 3.2.1.3, Marfan's syndrome and *HTRA1*-related SVDs share the common denominator of TGF-β signaling pathway dysregulation. Specifically in Marfan's syndrome, there is a pathological over-activation of TGF-β signaling in aortic VSMC leading to a pathological cell phenotype. This phenotypic switch is reversed upon overexpression of Klf4 (Dale et al., 2017), providing further evidence for a regulatory feedback mechanism relevant for vascular cell differentiation.

Lastly, cerebral cavernous malformations (CCMs) represent another cerebrovascular pathology where highly elevated Klf4 levels play a crucial role in disease pathogenesis, ultimately leading to clinical manifestations such as cerebral vessel malformations and markedly increased risk of intracerebral hemorrhage (Zhou et al., 2016). TGF-β signaling dysregulation is also implicated as a contributor of CCMs through promotion of epithelial–mesenchymal transition (EMT) (Cuttano et al., 2016).

Altogether, there is ample evidence to demonstrate interaction between TGF-β and Klf4. Furthermore, both have been identified to be decisive factors in the pathogenesis of

a number of vascular disorders. In the context of *HTRA1*-related SVDs, further research should be undertaken to identify the degree and mechanism(s) through which Klf4, TGF-β and shared signaling pathways contribute to disease development and progression.

6.3 Homozygous and Heterozygous *HTRA1* Mutations

CARASIL has been described as a strictly recessive disorder. However, over the course of this thesis I have consistently identified various pathological alterations in heterozygous *HTRA1* mutation carrier cells. My data thus suggest that *HTRA1* heterozygosity might be pathogenic. In good agreement, several studies have reported heterozygous *HTRA1* mutations in up to 5 % of patients suffering from familial SVD of unknown etiology (Verdura et al., 2015; Nozaki et al., 2016). These findings will further motivate screening efforts for *HTRA1* mutations in patients with SVD, lead to the identification of further cases, and thus stimulate interest in the pathobiological role of *HTRA1*.

In homozygous carrier cells, the majority of results showed a clear trend, but did not reach significance. This might be due to small sample size (3 homozygous cultures) and ongoing collection of additional patient cell cultures will help clarifying this point. Featuring a later age of onset and a lack of extraneurological symptoms, heterozygous patients display a milder phenotype than CARASIL cases. This suggests haploinsufficiency, i.e., a clinical phenotype based solely on the lack of functional protein from the defective allele, resulting in a lower total amount of intact gene product.

Alternatively, *HTRA1* mutations might display dominant-negative behavior. Indeed, HTRA1 assembles as a trimer to form a mature and proteolytically active complex (Clausen et al., 2011). In a heterozygous situation, mutant HTRA1 might thus neutralize up to two units of wild type HTRA1 within heterotrimers (see Figure 6.2). This possibility is supported by recent *in vitro* findings (Uemura et al., 2019; Nozaki et al., 2015). This type of pathomechanism has been extensively investigated for other SVD-related mutations targeting the multimeric protein type IV collagen (Gould et al. (2005), see Section 3.1.5). Analysis of the molecular (e.g., TGF-β signaling) and functional (e.g., vascular tone) phe-

notype in mouse models either deficient for *HTRA1* or bearing a pathogenic mutation could shed further light on this issue, when comparing homo- and heterozygous animals.

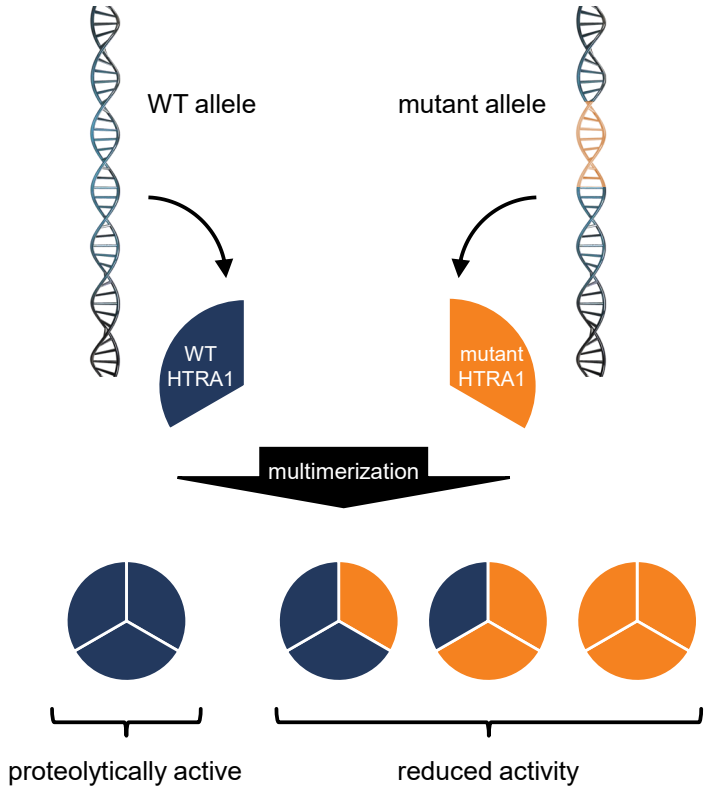

Figure 6.2.: Model for a dominant-negative effect of mutant HTRA1

Following transcription and translation, WT and mutant HTRA1, as found in a heterozygous mutation carrier, trimerize. The presence of mutant HTRA1 within the resulting heterotrimers might be sufficient to alter the global activity of the complex, resulting in a dominant-negative effect.

Remarkably, both the loss of contractile phenotype (as described in Section 5.2) and the switch towards a phagocytic expression pattern (see Section 5.3) observed on a molecular and/or functional level were generally more pronounced in heterozygous than in homozygous mutation carriers, clearly contrasting the clinical phenotype. One factor that may

have contributed to these findings is the small sample size of this study, especially regarding homozygous patients. Moreover, among the CARASIL patients, one individual (Pat3; see Table 4.1) presented a relatively late onset of clinical symptoms. Correspondingly, the expression pattern and contractile function observed for cultured fibroblasts of this individual was consistently less aberrant than that of the other two CARASIL patient samples.

6.4 Rescue Strategies

As an attempt to rescue cell phenotype I stimulated patient fibroblasts with recombinant TGF-β, resulting in upregulation of contraction marker expression and an improved cell contractility (see Section 5.6). While there is evidence to suggest that TGF-β may for instance suppress expression of galectin-3 (Tian et al., 2016), impact of this treatment on other markers including phagocytosis-associated markers and Klf4 in contractile cells remains to be investigated.

Successful TGF-β-induced rescue indicates that pathogenic phenotypic switching as observed in patient cells is not irreversible, hence providing the groundwork for the exploration of potential treatment strategies. However, not only is TGF-β a major contributing factor in fibrosis, mostly through upregulation of ECM production (Rockey et al., 2015), but it also plays a decisive role in various malignant diseases, where it for instance promotes EMT (Ikushima and Miyazono, 2010).

Thus, the exploration of alternative, more selective targets is of high interest. These might include components of the contractile apparatus. Yet again, known stimulators of contractile protein expression are mostly limited to growth factors, many of them associated with negative side effects comparable to those of TGF-β.

Modulation of so-called micro RNAs (miRNAs) might represent another promising strategy. miRNAs, which were first described in the early 2000s, are nucleotide sequences with a length of approximately 22 nucleotides. miRNAs regulate biological processes through the cleavage or transcriptional repression of mRNAs (see Figure 6.3). They are involved in numerous pathophysiological processes, and are emerging as valuable drug targets, inclu-

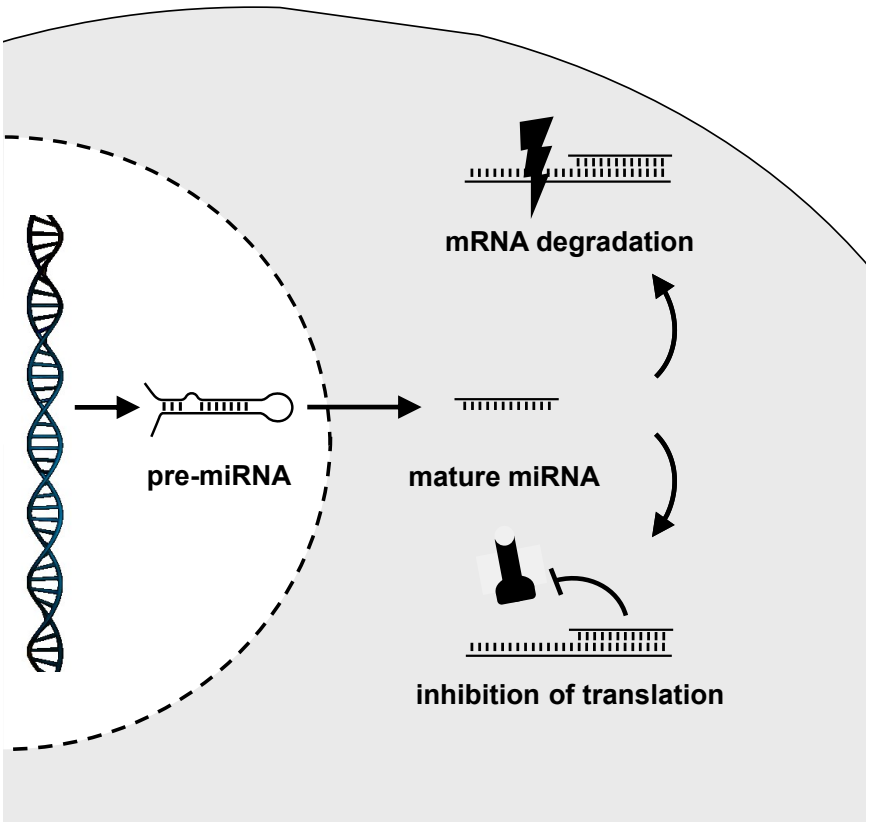

Figure 6.3.: miRNA-mediated regulation of cell phenotype

In the nucleus, RNA polymerase II transcribes primary (pri-)miRNA which is subsequently processed into pre-miRNA and transferred into the cytoplasm. There, processing through enzymatic cleavage yields mature, biologically active miRNA that may affect protein expression either through mRNA degradation or transcritptional repression (Kang and Hata, 2012). Elements of this Figure produced by Philippe Hupé and shared on `commons.wikimedia.org`

ding in the modulation of VSMC phenotype (Bartel, 2004). Notably, several miRNAs have been shown to specifically promote either the synthetic/proliferative (e.g. miRNAs 24; 31; 208 and 221) or the contractile VSMC phenotype (e.g. miRNAs 10a; 21; 143 and 145 as depicted in Figure 6.4) (Kang and Hata, 2012). Moreover, in the context of atherosclerosis in metabolic syndrome, treatment with miRNA 145 applied via an adenoviral vector successfully restored the contractile VSMC phenotype (Hutcheson et al., 2013).

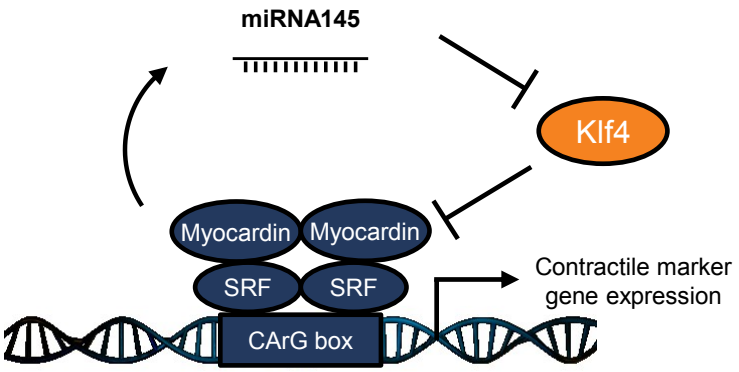

Figure 6.4.: miRNA 145 promotes the contractile expression program

The expression of miRNA 145, one of the best-described miRNAs involved in the maintenance of the contractile VSMC phenotype, is promoted by the SRF-myocardin transcriptional complex. One of its key mechanisms of action is the inhibition of Klf4, thus lifting Klf4-mediated suppression of the contractile gene expression program. For a more detailed illustration of Klf4-mediated inhibition of the SRF-myocardin complex, see Figure 3.9. Figure modelled after an illustration by Joshi et al. (2012).

Therefore, targeting these miRNAs might represent a suitable approach to rescue contractility, while leaving ECM deposition unaffected.

A Appendix: Methods

Background information on genotyping (Figure A.1), immunoblot (Figure A.2), immunohistochemistry (Figure A.3) and RT-qPCR (Figure A.4) experiments as elaborated in Chapter 4 is provided on the following pages.

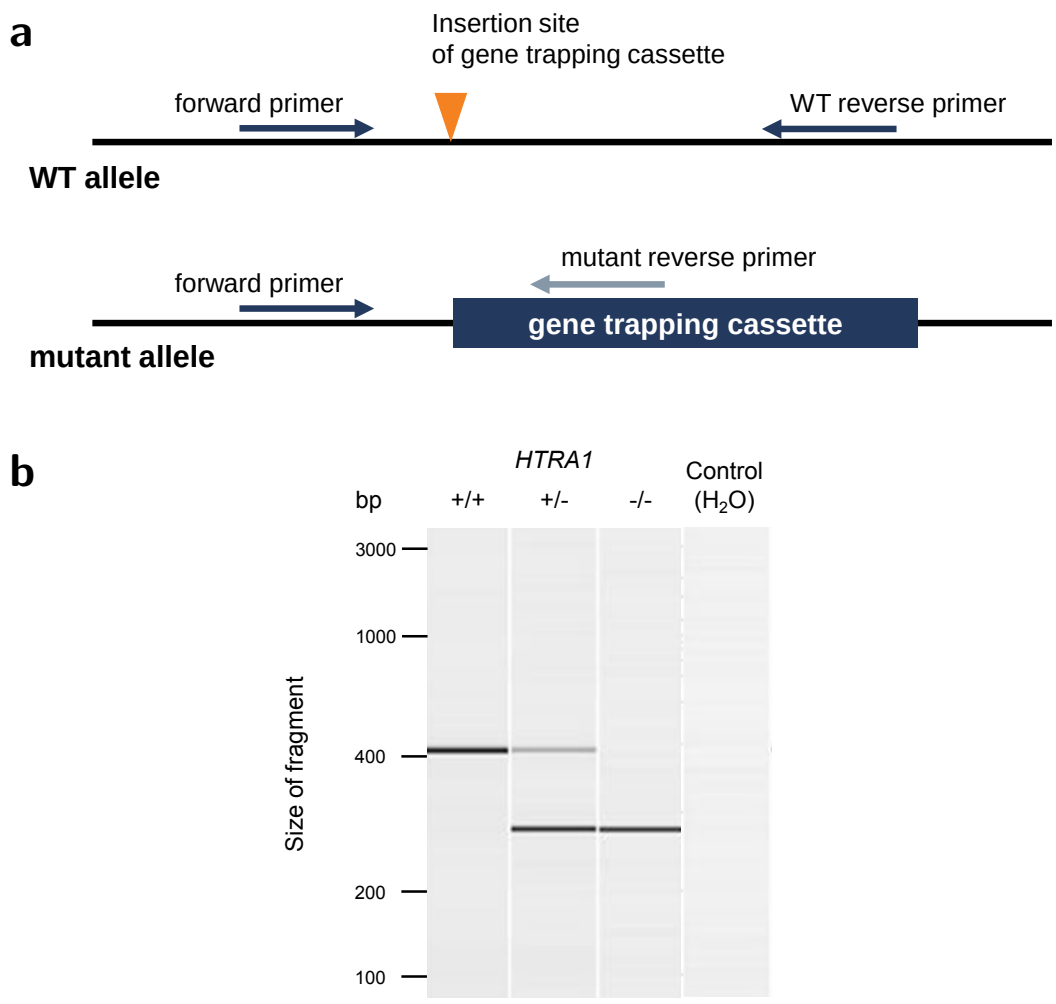

Figure A.1.: Genotyping of *HTRA1*$^{+/+}$, $^{+/-}$ and $^{-/-}$ mice

(**a**) Structure of the mouse *HTRA1* gene before and after gene trapping (WT and mutant allele, respectively). Arrows indicate the position of the genotyping primers. (**b**) Genotyping as performed with DNA from *HTRA1*$^{+/+}$, $^{+/-}$ and $^{-/-}$ animals. A DNA-free sample was included as control. Amplification of the WT allele produces a 434-bp fragment, while amplification of the mutant allele yields a 281-bp PCR product.

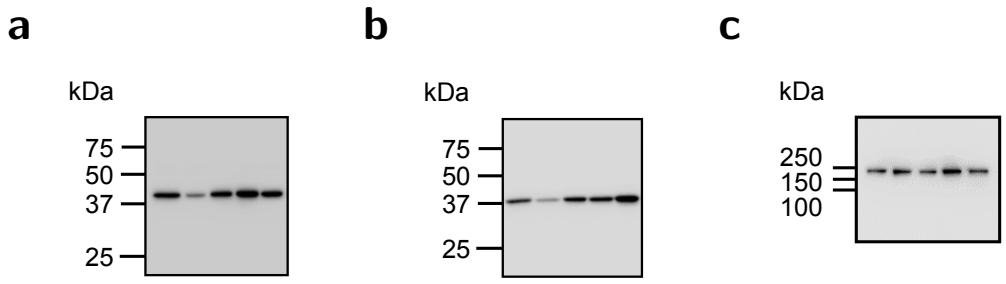

Figure A.2.: Antibody testing for immunoblot

Example featuring mouse full brain lysates analyzed by immunoblot using primary antibodies against (**a**) α-SMA (expected molecular mass 42 kDa), (**b**) calponin-1 (expected molecular mass 34 kDa), and (**c**) PDGFR-β (expected molecular mass 190 kDa).

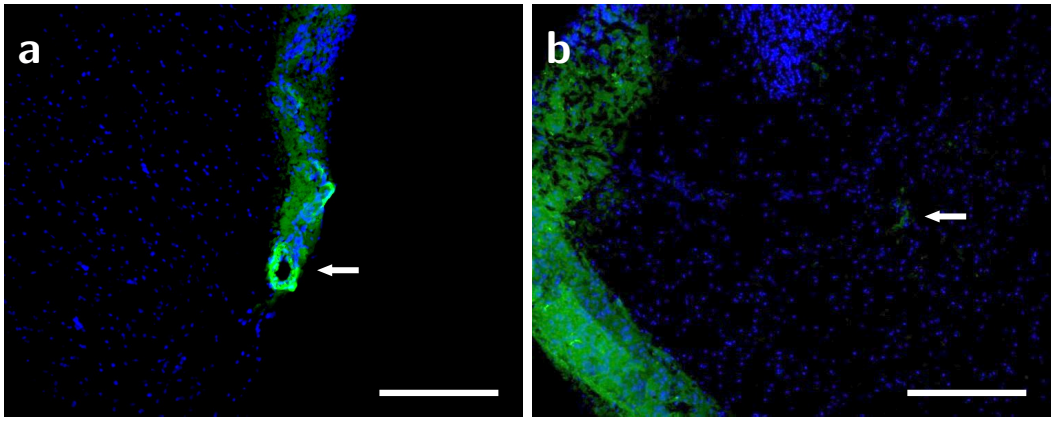

Figure A.3.: Antibody testing for immunohistochemistry

(**a**) Mouse brain sections were analyzed by immunohistochemistry using an anti-calponin antibody followed by detection with fluorophore-coupled anti-rabbit immunoglobulin antibody (green). In (**b**), the primary antibody was omitted. Nuclei were stained with DAPI (blue). Vessels with a diameter of approximately 50 µm are present in both sections (arrows). Scale bars represent 200 µm.

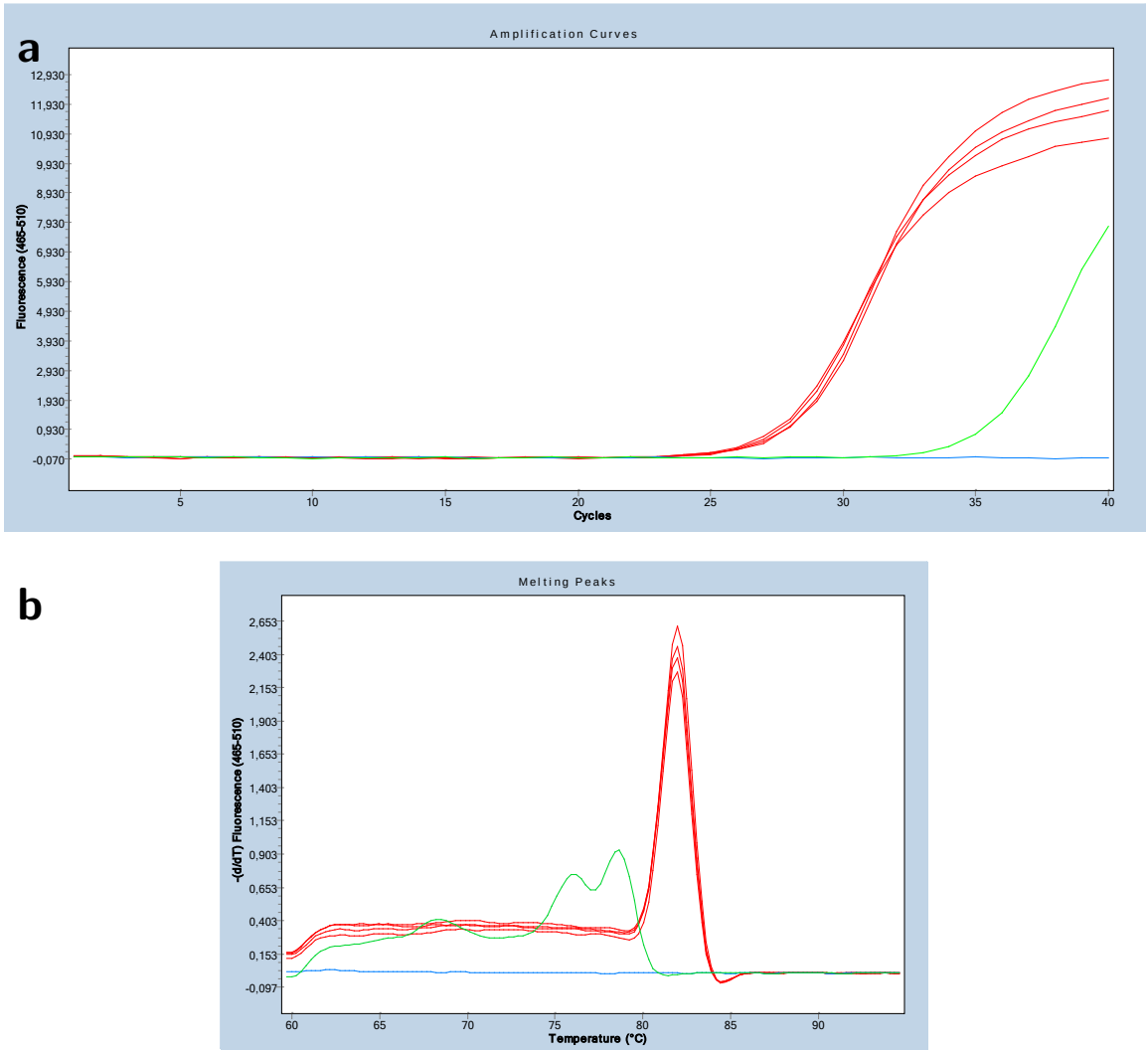

Figure A.4.: Primer testing for RT-qPCR

Human skin fibroblasts were analyzed for calponin (*CNN1*) expression by RT-qPCR. Red: cDNA (n = 2 samples; in duplicate); green: water control; blue: non-reverse transcribed control. (**a**) Amplification curves, showing C_T values of about 27 (C_T values > 35 indicate very low cDNA abundance). (**b**) Melting profiles, showing a sharp, single peak. Double peaks are commonly observed in water controls and correspond to primer dimers.

B Copyright Declaration

All figures for which no source information is provided are my own work. Figure 3.6 has been published under a creative commons license by its respective authors, who are stated in the figure's captions, and to whom I am very grateful for choosing this means of rights management. Permission for the reproduction of all other figures as listed in Table B.1 has been obtained through RightsLink[1].

Figure(s)	Author(s)	Publisher	License Nr.
3.1	Wardlaw et al. (2013)	Elsevier, Inc.	4403001365242
3.2	Wardlaw et al. (2013)	Elsevier, Inc.	3670270016661
3.4A	Menezes Cordeiro et al. (2015)	Wolters Kluwer Health, Inc.	3670251018554
3.4C	Fukutake (2011)	Elsevier, Inc.	3672980089399
3.4D; 3.4E	Oide et al. (2008)	John Wiley and Sons, Inc.	3670260252301

Table B.1.: License Numbers and copyright holders for all figures with copyright management via RightsLink

[1] http://www.copyright.com/rightsholders/rightslink-permissions/

C Bibliography

Arima, K., Yanagawa, S., Ito, N., and Ikeda, S. (2003). Cerebral arterial pathology of CADASIL and CARASIL (Maeda syndrome). *Neuropathology*, 23(4):327–334.

Assinder, S. J., Stanton, J.-a. L., and Prasad, P. D. (2009). Transgelin: An actin-binding protein and tumour suppressor. *The International Journal of Biochemistry & Cell Biology*, 41(3):482–486.

Balbi, M., Koide, M., Wellman, G. C., and Plesnila, N. (2017). Inversion of neurovascular coupling after subarachnoid hemorrhage in vivo. *Journal of Cerebral Blood Flow and Metabolism*, 37(11):3625–3634.

Bartel, D. P. (2004). MicroRNAs: Genomics, Biogenesis, Mechanism, and Function. *Cell*, 116(2):281–297.

Bayrakli, F., Balaban, H., Gurelik, M., Hizmetli, S., and Topaktas, S. (2014). Mutation in the HTRA1 gene in a patient with degenerated spine as a component of CARASIL syndrome. *Turkish Neurosurgery*, 24(1):67–69.

Beaufort, N., Scharrer, E., Kremmer, E., Lux, V., Ehrmann, M., Huber, R., Houlden, H., Werring, D., Haffner, C., and Dichgans, M. (2014). Cerebral small vessel disease-related protease HtrA1 processes latent TGF-β binding protein 1 and facilitates TGF-β signaling. *Proceedings of the National Academy of Sciences*, 111(46):16496–16501.

Bentov, I. and Reed, M. J. (2015). The effect of aging on the cutaneous microvasculature. *Microvascular Research*, 100(5 Pt 1):25–31.

Bianchi, S., Palma, C. D., Gallus, G., and Taglia, I. (2014). Two novel HTRA1 mutations in a European CARASIL patient. *Neurology*, 82(10):898–900.

Bougea, A., Velonakis, G., Spantideas, N., Anagnostou, E., Paraskevas, G., Kapaki, E., and Kararizou, E. (2017). The first Greek case of heterozygous cerebral autosomal recessive arteriopathy with subcortical infarcts and leukoencephalopathy: An atypical clinico-radiological presentation. *Neuroradiology Journal*, 30(6):583–585.

Buchwalter, G., Gross, C., and Wasylyk, B. (2004). Ets ternary complex transcription factors. *Gene*, 324(1-2):1–14.

Cen, B., Selvaraj, A., and Prywes, R. (2004). Myocardin/MKL family of SRF coactivators: Key regulators of immediate early and muscle specific gene expression. *Journal of Cellular Biochemistry*, 93(1):74–82.

Chabriat, H., Joutel, A., Dichgans, M., Tournier-Lasserve, E., and Bousser, M.-G. G. (2009). CADASIL. *The Lancet Neurology*, 8(7):643–653.

Chen, L., DeWispelaere, A., Dastvan, F., Osborne, W. R., Blechner, C., Windhorst, S., and Daum, G. (2016). Smooth muscle-alpha actin inhibits vascular smooth muscle cell proliferation and migration by inhibiting rac1 activity. *PLoS ONE*, 11(5):1–10.

Chen, Y., He, Z., Meng, S., Li, L., Yang, H., and Zhang, X. (2013). A novel mutation of the high-temperature requirement A serine peptidase 1 (HTRA1) gene in a Chinese family with cerebral autosomal recessive arteriopathy with subcortical infarcts and leukoencephalopathy (CARASIL). *Journal of International Medical Research*, 41(5):1445–1455.

Clausen, T., Kaiser, M., Huber, R., and Ehrmann, M. (2011). HTRA proteases: regulated proteolysis in protein quality control. *Nature Reviews Molecular Cell Biology*, 12(3):152–162.

Craggs, L. J., Yamamoto, Y., Deramecourt, V., and Kalaria, R. N. (2014). Microvascular Pathology and Morphometrics of Sporadic and Hereditary Small Vessel Diseases of the Brain. *Brain Pathology*, 24(5):495–509.

Cuttano, R., Rudini, N., Bravi, L., Corada, M., Giampietro, C., Papa, E., Morini, M. F., Maddaluno, L., Baeyens, N., Adams, R. H., Jain, M. K., Owens, G. K., Schwartz, M., Lampugnani, M. G., and Dejana, E. (2016). KLF 4 is a key determinant in the development and progression of cerebral cavernous malformations . *EMBO Molecular Medicine*, 8(1):6–24.

Dale, M., Fitzgerald, M. P., Liu, Z., Meisinger, T., Karpisek, A., Purcell, L. N., Carson, J. S., Harding, P., Lang, H., Koutakis, P., Batra, R., Mietus, C. J., Casale, G., Pipinos, I., Baxter, B. T., and Xiong, W. (2017). Premature aortic smooth muscle cell differentiation contributes to matrix dysregulation in Marfan Syndrome. *PLoS ONE*, 12(10):1–18.

de Groof, F. (2008). Extensive cerebral infarction in the newborn due to incontinentia pigmenti. *European Journal of Pediatric Neurology*, 12:284–289.

Dennler, S., Itoh, S., Vivien, D., ten Dijke, P., Huet, S., and Gauthier, J. M. (1998). Direct binding of Smad3 and Smad4 to critical TGF beta-inducible elements in the promoter of human plasminogen activator inhibitor-type 1 gene. *The EMBO journal*, 17(11):3091–100.

Diakiw, S. M., D'Andrea, R. J., and Brown, A. L. (2013). The double life of KLF5: Opposing roles in regulation of gene-expression, cellular function, and transformation. *IUBMB Life*, 65(12):999–1011.

Dichgans, M. (2002). CADASIL: A Monogenic Condition Causing Stroke and Subcortical Vascular Dementia. *Cerebrovascular Diseases*, 13(Suppl. 2):37–41.

Dichgans, M. (2007). Genetics of ischaemic stroke. *The Lancet Neurology*, 6(2):149–161.

Diwan, A. G., Bhosle, D. G., Vikram, A., Biniwale, A., Chaudhary, S., and Patodiya, B. (2012). CARASIL. *The Journal of the Association of Physicians of India*, 60:59–61.

Duering, M., Csanadi, E., Gesierich, B., Jouvent, E., Hervé, D., Seiler, S., Belaroussi, B., Ropele, S., Schmidt, R., Chabriat, H., and Dichgans, M. (2013). Incident lacunes

preferentially localize to the edge of white matter hyperintensities: insights into the pathophysiology of cerebral small vessel disease. *Brain*, 136(9):2717–2726.

Duering, M., Gesierich, B., Seiler, S., Pirpamer, L., Gonik, M., Hofer, E., Jouvent, E., Duchesnay, E., Chabriat, H., Ropele, S., Schmidt, R., and Dichgans, M. (2014). Strategic white matter tracts for processing speed deficits in age-related small vessel disease. *Neurology*, 82(22):1946–1950.

Duering, M., Zieren, N., Herve, D., Jouvent, E., Reyes, S., Peters, N., Pachai, C., Opherk, C., Chabriat, H., and Dichgans, M. (2011). Strategic role of frontal white matter tracts in vascular cognitive impairment: a voxel-based lesion-symptom mapping study in CADASIL. *Brain*, 134(8):2366–2375.

Feil, S., Fehrenbacher, B., Lukowski, R., Essmann, F., Schulze-Osthoff, K., Schaller, M., and Feil, R. (2014). Transdifferentiation of vascular smooth muscle cells to macrophage-like cells during atherogenesis. *Circulation Research*, 115(7):662–667.

Fukutake, T. (2011). Cerebral autosomal recessive arteriopathy with subcortical infarcts and leukoencephalopathy (CARASIL): From discovery to gene identification. *Journal of Stroke and Cerebrovascular Diseases*, 20(2):85–93.

Gaarenstroom, T. and Hill, C. S. (2014). TGF-β signaling to chromatin: How Smads regulate transcription during self-renewal and differentiation. *Seminars in Cell and Developmental Biology*, 32:107–118.

Gomez, D. and Owens, G. K. (2012). Smooth muscle cell phenotypic switching in atherosclerosis. *Cardiovascular Research*, 95(2):156–164.

Gomez, D., Shankman, L. S., Nguyen, A. T., and Owens, G. K. (2013). Detection of histone modifications at specific gene loci in single cells in histological sections. *Nature Methods*, 10(2):171–177.

Gould, D. B., Phalan, F. C., Breedveld, G. J., Van Mil, S. E., Smith, R. S., Schimenti, J. C., Aguglia, U., Van Der Knaap, M. S., Heutink, P., and John, S. W. (2005). Mutations in

Col4a1 cause perinatal cerebral hemorrhage and porencephaly. *Science*, 308(5725):1167–1171.

Haffner, C., Malik, R., and Dichgans, M. (2016). Genetic factors in cerebral small vessel disease and their impact on stroke and dementia. *Journal of Cerebral Blood Flow & Metabolism*, 36(1):158–171.

Hara, K., Shiga, A., Fukutake, T., Nozaki, H., Miyashita, A., Yokoseki, A., Kawata, H., Koyama, A., Arima, K., Takahashi, T., Ikeda, M., Shiota, H., Tamura, M., Shimoe, Y., Hirayama, M., Arisato, T., Yanagawa, S., Tanaka, A., Nakano, I., Ikeda, S.-i., Yoshida, Y., Yamamoto, T., Ikeuchi, T., Kuwano, R., Nishizawa, M., Tsuji, S., and Onodera, O. (2009). Association of HTRA1 Mutations and Familial Ischemic Cerebral Small-Vessel Disease. *New England Journal of Medicine*, 360(17):1729–1739.

Hu, B., Wu, Z., Liu, T., Ullenbruch, M. R., Jin, H., and Phan, S. H. (2007). Gut-Enriched Krüppel-Like Factor Interaction with Smad3 Inhibits Myofibroblast Differentiation. *American Journal of Respiratory Cell and Molecular Biology*, 36(1):78–84.

Hutcheson, R., Terry, R., Chaplin, J., Smith, E., Musiyenko, A., Russell, J. C., Lincoln, T., and Rocic, P. (2013). MicroRNA-145 restores contractile vascular smooth muscle phenotype and coronary collateral growth in the metabolic syndrome. *Arteriosclerosis, Thrombosis, and Vascular Biology*, 33(4):727–736.

Hynes, R. O. (2009). The extracellular matrix: not just pretty fibrils. *Science*, 326(5957):1216–1219.

Ikawati, M., Kawaichi, M., and Oka, C. (2018). Loss of HtrA1 serine protease induces synthetic modulation of aortic vascular smooth muscle cells. *PLoS ONE*, 13(5):1–22.

Ikushima, H. and Miyazono, K. (2010). TGFB 2 signalling: A complex web in cancer progression. *Nature Reviews Cancer*, 10(6):415–424.

Ishtiaq Ahmed, A. S., Bose, G. C., Huang, L., and Azhar, M. (2014). Generation of mice carrying a knockout-first and conditional-ready allele of transforming growth factor beta2 gene. *Genesis*, 52(9):817–826.

Iyemere, V. P., Proudfoot, D., Weissberg, P. L., and Shanahan, C. M. (2006). Vascular smooth muscle cell phenotypic plasticity and the regulation of vascular calcification. *Journal of Internal Medicine*, 260(3):192–210.

Jackson, C. and Sudlow, C. (2005). Comparing risks of death and recurrent vascular events between lacunar and non-lacunar infarction. *Brain*, 128(11):2507–2517.

Joshi, S. R., Comer, B. S., McLendon, J. M., and Gerthoffer, W. T. (2012). MicroRNA Regulation of Smooth Muscle Phenotype. *Molecular and Cellular Pharmacology*, 4(1):1–16.

Joutel, A., Corpechot, C., Ducros, A., Vahedi, K., Chabriat, H., Mouton, P., Alamowitch, S., Domenga, V., Cécillion, M., Maréchal, E., Maciazek, J., Vayssière, C., Cruaud, C., Cabanis, E.-A. A., Ruchoux, M. M., Weissenbach, J., Bach, J. F., Bousser, M. G., Tournier-Lasserve, E., Marechal, E., Maciazek, J., Vayssiere, C., Cruaud, C., Cabanis, E.-A. A., Ruchoux, M. M., Weissenbach, J., Bach, J. F., Bousser, M. G., and Tournier-Lasserve, E. (1996). Notch3 mutations in CADASIL, a hereditary adult-onset condition causing stroke and dementia. *Nature*, 383(6602):707–710.

Joutel, A. and Faraci, F. M. (2014). Cerebral Small Vessel Disease: Insights and Opportunities From Mouse Models of Collagen IV-Related Small Vessel Disease and Cerebral Autosomal Dominant Arteriopathy With Subcortical Infarcts and Leukoencephalopathy. *Stroke*, 45(4):1215–1221.

Kang, H. and Hata, A. (2012). MicroRNA regulation of smooth muscle gene expression and phenotype. *Current Opinion in Hematology*, 19(3):224–231.

Kast, J., Hanecker, P., Beaufort, N., Giese, A., Joutel, A., Dichgans, M., Opherk, C., and

Haffner, C. (2014). Sequestration of latent TGF-β binding protein 1 into CADASIL-related Notch3-ECD deposits. *Acta Neuropathologica Communications*, 2(1):96.

Khaleeli, Z., Jaunmuktane, Z., Beaufort, N., Houlden, H., Haffner, C., Brandner, S., Dichgans, M., and Werring, D. (2015). A novel HTRA1 exon 2 mutation causes loss of protease activity in a Pakistani CARASIL patient. *Journal of Neurology*, 262(5):1369–1372.

Kim, H. J., Kim, J. G., Moon, M. Y., Park, S. H., and Park, J. B. (2014). IκB kinase γ/nuclear factor-κB-essential modulator (IKKγ/NEMO) facilitates RhoA GTPase activation, which, in turn, activates Rho-associated kinase (ROCK) to phosphorylate IKKβ in response to transforming growth factor (TGF)-β1. *Journal of Biological Chemistry*, 289(3):1429–1440.

Kohn, J. C., Lampi, M. C., and Reinhart-King, C. A. (2015). Age-related vascular stiffening: causes and consequences. *Frontiers in Genetics*, 6(March):1–17.

Kurpinski, K., Lam, H., Chu, J., Wang, A., Kim, A., Tsay, E., Agrawal, S., Schaffer, D. V., and Li, S. (2010). Transforming Growth Factor-β and Notch Signaling Mediate Stem Cell Differentiation into Smooth Muscle Cells. *Stem Cells*, 28(4):734–742.

Lanfranconi, S. and Markus, H. S. (2010). COL4A1 mutations as a monogenic cause of cerebral small vessel disease: A systematic review. *Stroke*, 41(8):e513–e518.

Liu, Y., Sinha, S., and Owens, G. (2003). A Transforming Growth Factor-β Control Element Required for SM α-Actin Expression in Vivo Also Partially Mediates GKLF-dependent Transcriptional Repression. *Journal of Biological Chemistry*, 278(48):48004–48011.

Long, X., Bell, R. D., Gerthoffer, W. T., Zlokovic, B. V., and Miano, J. M. (2008). Myocardin Is Sufficient for a Smooth Muscle-Like Contractile Phenotype. *Arteriosclerosis, Thrombosis, and Vascular Biology*, 28(8):1505–1510.

MacCarrick, G., Black, J. H., Bowdin, S., El-Hamamsy, I., Frischmeyer-Guerrerio, P. A., Guerrerio, A. L., Sponseller, P. D., Loeys, B., and Dietz, H. C. (2014). Loeys–Dietz syndrome: a primer for diagnosis and management. *Genetics in Medicine*, 16(8):576–587.

Maeda, S., Nakayama, H., Isaka, K., Aihara, Y., and Nemoto, S. (1976). Familial unusual encephalopathy of Binswanger's type without hypertension. *Folia psychiatrica et neurologica japonica*, 30(2):165–177.

Massagué, J. (2012). TGFβ signalling in context. *Nature Reviews Molecular Cell Biology*, 13(10):616–630.

Mcconnell, B. B. and Yang, V. W. (2010). Mammalian Krueppel-Like Factors in Health and Diseases. *Physiological Reviews*, 90(361):1337–1381.

McDonald, O. G., Wamhoff, B. R., Hoofnagle, M. H., and Owens, G. K. (2006). Control of SRF binding to CArG box chromatin regulates smooth muscle gene expression in vivo. *Journal of Clinical Investigation*, 116(1):36–48.

Mehta, A., Ricci, R., Widmer, U., Dehout, F., Garcia de Lorenzo, A., Kampmann, C., Linhart, A., Sunder-Plassmann, G., Ries, M., and Beck, M. (2004). Fabry disease defined: baseline clinical manifestations of 366 patients in the Fabry Outcome Survey. *European Journal of Clinical Investigation*, 34(3):236–242.

Menezes Cordeiro, I., Nzwalo, H., Sá, F., Ferreira, R. B., Alonso, I., Afonso, L., Basílio, C., Sa, F., Ferreira, R. B., Alonso, I., Afonso, L., and Basilio, C. (2015). Shifting the CARASIL Paradigm: Report of a Non-Asian Family and Literature Review. *Stroke*, 46(4):1110–1112.

Miano, J. M. (2003). Serum response factor: Toggling between disparate programs of gene expression. *Journal of Molecular and Cellular Cardiology*, 35(6):577–593.

Miano, J. M. (2015). Myocardin in biology and disease. *Journal of Biomedical Research*, 29(1):3–19.

Milewicz, D. M., Guo, D.-C., Tran-Fadulu, V., Lafont, A. L., Papke, C. L., Inamoto, S., Kwartler, C. S., and Pannu, H. (2008). Genetic Basis of Thoracic Aortic Aneurysms and Dissections: Focus on Smooth Muscle Cell Contractile Dysfunction. *Annual Review of Genomics and Human Genetics*, 9(1):283–302.

Mok, V. and Kim, S. (2015). Prevention and Management of Cerebral Small Vessel Disease. *Journal of Stroke*, 17(2):111–122.

Monet-Leprêtre, M., Haddad, I., Baron-Menguy, C., Fouillot-Panchal, M., Riani, M., Domenga-Denier, V., Dussaule, C., Cognat, E., Vinh, J., and Joutel, A. (2013). Abnormal recruitment of extracellular matrix proteins by excess Notch3ECD: a new pathomechanism in CADASIL. *Brain*, 136(6):1830–1845.

Mullen, A. C., Orlando, D. A., Newman, J. J., Lovén, J., Kumar, R. M., Bilodeau, S., Reddy, J., Guenther, M. G., DeKoter, R. P., and Young, R. A. (2011). Master Transcription Factors Determine Cell-Type-Specific Responses to TGF-β Signaling. *Cell*, 147(3):565–576.

Nozaki, H., Kato, T., Nihonmatsu, M., Saito, Y., Mizuta, I., Noda, T., Koike, R., Miyazaki, K., Kaito, M., Ito, S., Makino, M., Koyama, A., Shiga, A., Uemura, M., Sekine, Y., Murakami, A., Moritani, S., Hara, K., Yokoseki, A., Kuwano, R., Endo, N., Momotsu, T., Yoshida, M., Nishizawa, M., Mizuno, T., and Onodera, O. (2016). Distinct molecular mechanisms of HTRA1 mutants in manifesting heterozygotes with CARASIL. *Neurology*, 86(21):1964–1974.

Nozaki, H., Sekine, Y., Fukutake, T., Nishimoto, Y., Shimoe, Y., Shirata, A., Yanagawa, S., Hirayama, M., Tamura, M., Nishizawa, M., and Onodera, O. (2015). Characteristic features and progression of abnormalities on MRI for CARASIL. *Neurology*, 85(5):459–463.

Ohkuma, H., Suzuki, S., and Ogane, K. (2003). Phenotypic modulation of smooth muscle

cells and vascular remodeling in intraparenchymal small cerebral arteries after canine experimental subarachnoid hemorrhage. *Neuroscience Letters*, 344(3):193–196.

Oide, T., Nakayama, H., Yanagawa, S., Ito, N., Ikeda, S.-i. I., and Arima, K. (2008). Extensive loss of arterial medial smooth muscle cells and mural extracellular matrix in cerebral autosomal recessive arteriopathy with subcortical infarcts and leukoencephalopathy (CARASIL). *Neuropathology*, 28(2):132–142.

Owens, G. K., Kumar, M. S., and Wamhoff, B. R. (2004). Molecular Regulation of Vascular Smooth Muscle Cell Differentiation in Development and Disease. *Physiological Reviews*, 84(3):767–801.

Pantoni, L. (2010). Cerebral small vessel disease: from pathogenesis and clinical characteristics to therapeutic challenges. *The Lancet Neurology*, 9(7):689–701.

Pardali, E. (2012). TGFβ Signaling and Cardiovascular Diseases. *International Journal of Biological Sciences*, 8(April):195–213.

Potter, G. M., Doubal, F. N., Jackson, C. a., Chappell, F. M., Sudlow, C. L., Dennis, M. S., and Wardlaw, J. M. (2010). Counting cavitating lacunes underestimates the burden of lacunar infarction. *Stroke*, 41(2):267–272.

Potter, G. M., Doubal, F. N., Jackson, C. a., Chappell, F. M., Sudlow, C. L., Dennis, M. S., and Wardlaw, J. M. (2013). Enlarged perivascular spaces and cerebral small vessel disease. *International Journal of Stroke*, 10(April):376–381.

Rensen, S. S. M., Doevendans, P. A. F. M., and van Eys, G. J. J. M. (2007). Regulation and characteristics of vascular smooth muscle cell phenotypic diversity. *Netherlands Heart Journal*, 15(3):100–108.

Richards, A., van den Maagdenberg, A. M. J. M., Jen, J. C., Kavanagh, D., Bertram, P., Spitzer, D., Liszewski, M. K., Barilla-Labarca, M.-L., Terwindt, G. M., Kasai, Y., McLellan, M., Grand, M. G., Vanmolkot, K. R. J., de Vries, B., Wan, J., Kane, M. J.,

Mamsa, H., Schäfer, R., Stam, A. H., Haan, J., de Jong, P. T. V. M., Storimans, C. W., van Schooneveld, M. J., Oosterhuis, J. A., Gschwendter, A., Dichgans, M., Kotschet, K. E., Hodgkinson, S., Hardy, T. a., Delatycki, M. B., Hajj-Ali, R. A., Kothari, P. H., Nelson, S. F., Frants, R. R., Baloh, R. W., Ferrari, M. D., and Atkinson, J. P. (2007). C-terminal truncations in human 3'-5' DNA exonuclease TREX1 cause autosomal dominant retinal vasculopathy with cerebral leukodystrophy. *Nature Genetics*, 39(9):1068–70.

Rincon, F. and Wright, C. B. (2014). Current pathophysiological concepts in cerebral small vessel disease. *Frontiers in Aging Neuroscience*, 6(March):24.

Ringelstein, E. B., Kleffner, I., Dittrich, R., Kuhlenbäumer, G., and Ritter, M. a. (2010). Hereditary and non-hereditary microangiopathies in the young. An up-date. *Journal of the Neurological Sciences*, 299(1-2):81–85.

Rockey, D. C., Bell, P. D., and Hill, J. a. (2015). Fibrosis — A Common Pathway to Organ Injury and Failure. *New England Journal of Medicine*, 372(12):1138–1149.

Roeben, B., Uhrig, S., Bender, B., and Synofzik, M. (2016). Teaching neuro images: When alopecia and disk herniations meet vascular leukoencephalopathy. *Neurology*, 86(15):e166–e167.

Rong, J. X., Shapiro, M., Trogan, E., and Fisher, E. a. (2003). Transdifferentiation of mouse aortic smooth muscle cells to a macrophage-like state after cholesterol loading. *Proceedings of the National Academy of Sciences of the United States of America*, 100(23):13531–13536.

Rosenfeld, M. E. (2015). Converting smooth muscle cells to macrophage-like cells with KLF4 in atherosclerotic plaques. *Nature Medicine*, 21(6):549–551.

Salmon, M., Gomez, D., Greene, E., Shankman, L., and Owens, G. K. (2012). Cooperative Binding of KLF4, pELK-1, and HDAC2 to a G/C Repressor Element in the SM22α Promoter Mediates Transcriptional Silencing During SMC Phenotypic Switching In Vivo. *Circulation Research*, 111(6):685–696.

Schmittgen, T. D. and Livak, K. J. (2008). Analyzing real-time PCR data by the comparative CT method. *Nature Protocols*, 3(6):1101–1108.

Schnaper, H. W., Hayashida, T., and Poncelet, A.-C. (2002). It's a Smad world: regulation of TGF-beta signaling in the kidney. *Journal of the American Society of Nephrology : JASN*, 13(4):1126–1128.

Shankman, L. S., Gomez, D., Cherepanova, O. a., Salmon, M., Alencar, G. F., Haskins, R. M., Swiatlowska, P., Newman, A. a. C., Greene, E. S., Straub, A. C., Isakson, B., Randolph, G. J., and Owens, G. K. (2015). KLF4-dependent phenotypic modulation of smooth muscle cells has a key role in atherosclerotic plaque pathogenesis. *Nature Medicine*, 21(6):628–637.

Smahi, A., Courtois, G., Vabres, P., Yamaoka, S., Heuertz, S., Munnich, A., Israël, A., Heiss, N., Klauck, S., Kioschis, P., Wiemann, S., Poustka, A., Esposito, T., Bardaro, T., Gianfrancesco, F., Ciccodicola, A., D'Urso, M., Woffendin, H., Jakins, T., Donnai, D., Stewart, H., Kenwrick, S., Aradhya, S., Yamagata, T., Levy, M., Lewis, R., and Nelson, D. (2000). Genomic rearrangement in NEMO impairs NF- k B activation and is a cause of incontinentia pigmenti. *Nature*, 405(May):466–472.

Staals, J., Makin, S. D. J., Doubal, F. N., Dennis, M. S., and Wardlaw, J. M. (2014). Stroke subtype, vascular risk factors, and total MRI brain small-vessel disease burden. *Neurology*, 83(14):1228–34.

Sun, H., Peng, Z., Tang, H., Xie, D., Jia, Z., Zhong, L., Zhao, S., Ma, Z., Gao, Y., Zeng, L., Luo, R., and Xie, K. (2017). Loss of KLF4 and consequential downregulation of Smad7 exacerbate oncogenic TGF-β signaling in and promote progression of hepatocellular carcinoma. *Oncogene*, 36(21):2957–2968.

Sunaga, H., Matsui, H., Anjo, S., Syamsunarno, M. R. A., Koitabashi, N., Iso, T., Matsuzaka, T., Shimano, H., Yokoyama, T., and Kurabayashi, M. (2016). Elongation of long-chain fatty acid family member 6 (Elovl6)-driven fatty acid metabolism regulates

vascular smooth muscle cell phenotype through AMP-activated protein kinase/Krüppel-like factor 4 (AMPK/KLF4) signaling. *Journal of the American Heart Association*, 5(12):3–39.

Tan, R. Y. Y. and Markus, H. S. (2015). Monogenic causes of stroke: now and the future. *Journal of Neurology*, 262(12):2601–2616.

Thompson, C. S. and Hakim, A. M. (2009). Living beyond our physiological means: Small vessel disease of the brain is an expression of a systemic failure in arteriolar function: A unifying hypothesis. *Stroke*, 40(5):e322–30.

Tian, Y., Yuan, W., Li, J., Wang, H., Hunt, M. G., Liu, C., Shapiro, I. M., and Risbud, M. V. (2016). TGFβ regulates Galectin-3 expression through canonical Smad3 signaling pathway in nucleus pulposus cells: Implications in intervertebral disc degeneration. *Matrix Biology*, 50:39–52.

Uemura, M., Nozaki, H., Koyama, A., Sakai, N., Ando, S., Kanazawa, M., Kato, T., and Onodera, O. (2019). HTRA1 Mutations Identified in Symptomatic Carriers Have the Property of Interfering the Trimer-Dependent Activation Cascade. *Frontiers in Neurology*, 10(June):1–6.

Vahedi, K., Chabriat, H., Levy, C., Joutel, A., Tournier-Lasserve, E., and Bousser, M.-G. (2004). Migraine With Aura and Brain Magnetic Resonance Imaging Abnormalities in Patients With CADASIL. *Archives of Neurology*, 61(8):1237–40.

Vengrenyuk, Y., Nishi, H., Long, X., Ouimet, M., Savji, N., Martinez, F. O., Cassella, C. P., Moore, K. J., Ramsey, S. a., Miano, J. M., and Fisher, E. a. (2015). Cholesterol Loading Reprograms the MicroRNA-143/145–Myocardin Axis to Convert Aortic Smooth Muscle Cells to a Dysfunctional Macrophage-Like Phenotype. *Arteriosclerosis, Thrombosis, and Vascular Biology*, 35(3):535–546.

Verdura, E., Hervé, D., Scharrer, E., Amador, M. d. M., Guyant-Maréchal, L., Philippi, A., Corlobé, A., Bergametti, F., Gazal, S., Prieto-Morin, C., Beaufort, N., Le Bail, B.,

Viakhireva, I., Dichgans, M., Chabriat, H., Haffner, C., Tournier-Lasserve, E., Herve, D., Scharrer, E., Amador, M. d. M., Guyant-Marechal, L., Philippi, A., Corlobe, A., Bergametti, F., Gazal, S., Prieto-Morin, C., Beaufort, N., Le Bail, B., Viakhireva, I., Dichgans, M., Chabriat, H., Haffner, C., and Tournier-Lasserve, E. (2015). Heterozygous HTRA1 mutations are associated with autosomal dominant cerebral small vessel disease. *Brain*, 138(8):2347–2358.

Vizan, P., Miller, D. S. J., Gori, I., Das, D., Schmierer, B., and Hill, C. S. (2013). Controlling Long-Term Signaling: Receptor Dynamics Determine Attenuation and Refractory Behavior of the TGF- Pathway. *Science Signaling*, 6(305):ra106–ra106.

Wang, D.-Z., Li, S., Hockemeyer, D., Sutherland, L., Wang, Z., Schratt, G., Richardson, J. a., Nordheim, A., and Olson, E. N. (2002). Potentiation of serum response factor activity by a family of myocardin-related transcription factors. *Proceedings of the National Academy of Sciences of the United States of America*, 99(23):14855–14860.

Wang, G., Jacquet, L., Karamariti, E., and Xu, Q. (2015). Origin and differentiation of vascular smooth muscle cells. *The Journal of Physiology*, 593(14):3013–3030.

Wang, Z., Wang, D.-Z., Hockemeyer, D., McAnally, J., Nordheim, A., and Olson, E. N. (2004). Myocardin and ternary complex factors compete for SRF to control smooth muscle gene expression. *Nature*, 428(6979):185–189.

Wardlaw, J. M., Dennis, M. S., Warlow, C. P., and Sandercock, P. A. (2001). Imaging appearance of the symptomatic perforating artery in patients with lacunar infarction: Occlusion or other vascular pathology? *Annals of Neurology*, 50(2):208–215.

Wardlaw, J. M., Doubal, F., Armitage, P., Chappell, F., Carpenter, T., Muñoz Maniega, S., Farrall, A., Sudlow, C., Dennis, M., and Dhillon, B. (2009). Lacunar stroke is associated with diffuse blood-brain barrier dysfunction. *Annals of Neurology*, 65(2):194–202.

Wardlaw, J. M., Smith, C., and Dichgans, M. (2013). Mechanisms of sporadic cerebral small vessel disease: insights from neuroimaging. *The Lancet Neurology*, 12(5):483–497.

Yao, S., Tian, C., Ding, Y., Ye, Q., Gao, Y., Yang, N., and Li, Q. (2016). Down-regulation of Krüppel-like factor-4 by microRNA-135a-5p promotes proliferation and metastasis in hepatocellular carcinoma by transforming growth factor-β1. *Oncotarget*, 7(27):42566–42578.

Yoshida, T., Kaestner, K. H., and Owens, G. K. (2008). Conditional Deletion of Krüppel-Like Factor 4 Delays Downregulation of Smooth Muscle Cell Differentiation Markers but Accelerates Neointimal Formation Following Vascular Injury. *Circulation Research*, 102(12):1548–1557.

Zarate, Y. a. and Hopkin, R. J. (2008). Fabry's disease. *The Lancet*, 372(9647):1427–1435.

Zellner, A., Scharrer, E., Arzberger, T., Oka, C., Domenga-Denier, V., Joutel, A., Lichtenthaler, S. F., Müller, S. A., Dichgans, M., and Haffner, C. (2018). CADASIL brain vessels show a HTRA1 loss-of-function profile. *Acta Neuropathologica*, 136(1):111–125.

Zhang, X., Meng, H., Blaivas, M., Rushing, E. J., Moore, B. E., Schwartz, J., Lopes, M. B. S., Worrall, B. B., and Wang, M. M. (2012). von Willebrand Factor Permeates Small Vessels in CADASIL and Inhibits Smooth Muscle Gene Expression. *Translational Stroke Research*, 3(1):138–145.

Zhang, X.-h. H. X. X.-H., Zheng, B., Yang, Z., He, M., Yue, L.-y. Y., Zhang, R.-N. N., Zhang, M., Zhang, W., Zhang, X.-h. H. X. X.-H., and Wen, J.-k. K. (2015). TMEM16A and Myocardin Form a Positive Feedback Loop That Is Disrupted by KLF5 During Ang II-Induced Vascular Remodeling. *Hypertension*, 66(2):412–421.

Zheng, B., Han, M., and Wen, J.-K. K. (2010). Role of Krüppel-like factor 4 in phenotypic switching and proliferation of vascular smooth muscle cells. *IUBMB Life*, 62(2):132–139.

Zhou, J., Hu, G., and Herring, B. P. (2005). Smooth Muscle-Specific Genes Are Differentially Sensitive to Inhibition by Elk-1. *Molecular and Cellular Biology*, 25(22):9874–9885.

Zhou, Z., Tang, A. T., Wong, W. Y., Bamezai, S., Goddard, L. M., Shenkar, R., Zhou, S., Yang, J., Wright, A. C., Foley, M., Arthur, J. S. C., Whitehead, K. J., Awad, I. A., Li,

D. Y., Zheng, X., and Kahn, M. L. (2016). Cerebral cavernous malformations arise from endothelial gain of MEKK3-KLF2/4 signalling. *Nature*, 532(7597):122–126.

D Acknowledgements

First and foremost I would like to extend my sincere gratitude to Dr. Nathalie Beaufort. Without her unbreakable motivation, technical and educational support, and near-inexhaustible well of new ideas and directions, should something not work or turn out as planned, this thesis would have never come to life.

I would also like to thank PD Dr. Christof Haffner for his continued support and valuable input throughout this work and, similarly, Prof. Dr. Martin Dichgans, who has imbued the ISD and the *Translational Stroke and Dementia Research* group in particular with powerful ideas and resources.

I thoroughly enjoyed the working environment at the ISD, much owed to its fantastic team. Thank you, Dr. Farida Hellal, for heaps of scientific input, a contagious passion for science and ever so pleasant pre-judo-dinners at the ISD kitchen, Dr. Steffen Tiedt and Dr. Yaw Asare for input, technical support, and fruitful discussions spanning from small vessel disease to football. Thank you, Dr. Eva Scharrer, for laying the groundwork for this thesis together with Nathalie, and Dr. Matilde Balbi and Dr. Mitrajit Gosh for input and resources.

For their invaluable technical support, I would also like to thank Manuela Schneider, Natalie Leistner, and Barbara Lindner. I am also grateful to Dr. Manuela Schneider for her work and education regarding animal keeping.

This section would not be complete without acknowledging the Klinikum der Universität München and its FöFoLe program that accompanied me throughout this work with financial and educational support.

Last but certainly not least, I would like to thank the one person that has had the biggest influence on my life, from sparking an interest in education and science, fostering my hobbies and interests to providing me with endless patience, support, and life advice: Danke, Mama!